Global and Planetary Change 206 (2021) 103595

Contents lists available at ScienceDirect

Global and Planetary Change

journal homepage: www.elsevier.com/locate/gloplacha

Exploring the paleoceanographic changes registered by planktonic foraminifera across the Cenomanian-Turonian boundary interval and Oceanic Anoxic Event 2 at southern high latitudes in the Mentelle Basin (SE Indian Ocean)

Maria Rose Petrizzo [a,*], David K. Watkins [b], Kenneth G. MacLeod [c], Takashi Hasegawa [d], Brian T. Huber [e], Sietske J. Batenburg [f], Tomonori Kato [g]

[a] Dipartimento di Scienze della Terra "A. Desio", Università degli Studi di Milano, via Mangiagalli 34, 20133 Milano, Italy
[b] Department of Earth and Atmospheric Sciences, University of Nebraska, Lincoln, NE 68588, United States
[c] Department of Geological Sciences, University of Missouri-Columbia, Columbia, MO 65211, United States
[d] Department of Earth Sciences, Faculty of Natural Systems, Kanazawa University, Japan
[e] National Museum of Natural History, Smithsonian Institution, MRC-121, Washington, DC 20013, United States
[f] Departament de Dinàmica de la Terra i de l'Oceà, Facultat de Ciències de la Terra, Universitat de Barcelona, 08028 Barcelona, Spain
[g] Graduate School of Natural Science and Engineering, Kanazawa University, Japan

ARTICLE INFO

Keywords:
Planktonic foraminifera
Stable carbon and oxygen isotope
Oceanic Anoxic Event 2
Cenomanian/Turonian boundary
Paleoceanography
Southern high latitudes

ABSTRACT

Planktonic foraminiferal population dynamics and benthic foraminiferal and radiolaria distributions combined with $\delta^{13}C$ and $\delta^{18}O$ measurements of both bulk carbonate and foraminifera provide clues concerning the paleoceanographic changes across the Cenomanian-Turonian boundary interval and the Oceanic Anoxic Event 2 (OAE 2) at southern high latitudes. Samples analyzed are from Integrated Ocean Discovery Program (IODP) Expedition 369 Site U1516 in the Mentelle Basin (eastern flank of the Naturaliste Plateau, Indian Ocean, SW Australia). Site U1516 was located at 60°–62°S paleolatitude during the mid-Cretaceous, and it is the first high latitude locality in the Southern Hemisphere where planktonic foraminifera are consistently recorded across the OAE 2 interval and its associated positive $\delta^{13}C$ excursion.

The sedimentary record at Site U1516 consists of a sequence of alternating black, dark greenish gray, and light greenish gray claystone in the Cenomanian that grade to white and light gray calcareous chalk interbedded with chert in the Turonian. The correlation between the $\delta^{13}C$ and $\delta^{18}O$ profiles at Site U1516 and the European reference section at Eastbourne (England) coupled with the integrated calcareous plankton biostratigraphy and stable isotopic data at Site U1516, indicate that a complete record of OAE 2 at Site U1516 was recovered.

Below and in the lower part of OAE 2, the planktonic foraminiferal assemblages are dominated by small-sized (125–38 μm) opportunistic species of *Microhedbergella* and radiolaria indicating a dominantly eutrophic regime. Above the onset of OAE 2, a trough in the $\delta^{13}C$ profile (Plenus Carbon Isotope Event: P-CIE) coinciding with a $\delta^{18}O$ increase may correspond to the Plenus Cold Event as observed at low latitudes, although no evidence of cooling is registered in the microfossil assemblages. At Site U1516, the middle part of OAE 2 at the initiation of the plateau phase of the $\delta^{13}C$ profile is masked by absence of carbonate, by the highest TOC values, and high biogenic silica (dominance of radiolaria) indicating this interval corresponded to a time of highly stressed eutrophic conditions with possible shoaling of the Carbonate Compensation Depth (CCD). Above this interval, bulk isotopic results yield lower $\delta^{13}C$ values, and the $CaCO_3$ increases are associated with the presence of even smaller-sized *Microhedbergella* showing cyclic fluctuations in absolute abundances with benthic foraminifera indicating dominantly eutrophic conditions likely affected by upwelling of nutrient-rich and $\delta^{13}C$-depleted intermediate water masses. Toward the top of OAE 2 and across the Cenomanian-Turonian boundary interval, the planktonic foraminiferal assemblages show changes in composition (e.g., *Microhedbergella* is replaced by *Muricohedbergella*), species occupying relatively deep ecological niches appear and an overall increase in diversity is

* Corresponding author.
E-mail addresses: mrose.petrizzo@unimi.it (M.R. Petrizzo), dwatkins1@unl.edu (D.K. Watkins), macleodk@missouri.edu (K.G. MacLeod), jh7ujr@staff.kanazawa-u.ac.jp (T. Hasegawa), huberb@si.edu (B.T. Huber), sbatenburg@ub.edu (S.J. Batenburg), tomo1876@gmail.com (T. Kato).

https://doi.org/10.1016/j.gloplacha.2021.103595
Received 23 February 2021; Received in revised form 22 July 2021; Accepted 27 July 2021
Available online 6 August 2021

observed. These features coupled with the foraminiferal species-specific $\delta^{13}C$ and $\delta^{18}O$ patterns reveal that Site U1516 occupied a paleoceanographic setting still affected by eutrophy likely related to enhanced input of nutrients but with episodes of stability with ecological/thermal separation in the surface waters. This interval also records the highest sea surface water paleotemperatures values estimated as 20°–23°C based on $\delta^{18}O$ values of foraminiferal test and assuming seawater $\delta^{18}O$ values of $-1‰_{V\text{-}SMOW}$. Mesotrophic to oligotrophic conditions persisted after the OAE 2 and throughout the Turonian as evidenced by a diverse planktonic foraminiferal assemblage with different species occupying separate ecological niches in the mixed layer and thermocline.

1. Introduction

The Cenomanian-Turonian boundary interval and the perturbations associated with Oceanic Anoxic Event 2 (OAE 2, e.g., Schlanger and Jenkyns, 1976; Scholle and Arthur, 1980; Schlanger et al., 1987), provides a excellent opportunity to investigate the evolution of the marine biota in response to dramatic environmental perturbations. OAE 2 was a time of widespread change in the ventilation of the deep ocean and is associated with a perturbation of the global carbon cycle shown by a positive $\delta^{13}C$ excursion in marine and terrestrial records that resulted from the burial of large amounts of organic matter in deep-sea and hemipelagic settings (e.g., Scholle and Arthur, 1980; Tsikos et al., 2004; Voigt et al., 2006; Jenkyns, 2010; Wendler, 2013; Jenkyns et al., 2017). The event was probably triggered by a massive injection of CO_2 and nutrients into the ocean-atmosphere system through intense submarine volcanic activity and basalt-seawater interaction. A likely candidate for the volcanic event is the emplacement of the Caribbean Large Igneous Province and/or the High Arctic Large Igneous Province that emitted greenhouse gases and provided biolimiting metals in marine ecosystems leading to the onset of the Cenomanian-Turonian Thermal Maximum and the enhancement of ocean fertility (e.g., Larson, 1991; Kuypers et al., 2002; Leckie et al., 2002; Jenkyns, 2003; Erba, 2004; Pancost et al., 2004; Kuroda et al., 2007; Turgeon and Creaser, 2008; Barclay et al., 2010; Trabucho Alexandre et al., 2010; Zheng et al., 2013; Du Vivier et al., 2014; Scaife et al., 2017; Schröder-Adams et al., 2019).

Many hypotheses have been presented to account for increases in the global rate of organic-carbon burial during OAE 2 including eustatic sea-level rise that moved oxygen minimum zones onto the continental shelf (Schlanger and Jenkyns, 1976; Arthur et al., 1987; Gavrilov et al., 2013), increase in the flux of terrigenous nutrients to the oceans due to late Cenomanian sea-level rise (Erbacher et al., 2005; Bjerrum et al., 2006), input of volcanically derived nutrients to the oceans (Kerr, 1998; Larson and Erba, 1999; Turgeon and Creaser, 2008; Du Vivier et al., 2014; Jenkyns et al., 2017), changes in the cycling of major nutrients (Mort et al., 2007; Adams et al., 2010; Higgins et al., 2012), changes in ocean circulation (MacLeod et al., 2008; Martin et al., 2012; Zheng et al., 2013), CO_2-induced warming and increase in the delivery of weathering-derived nutrients to the oceans (Frijia and Parente, 2008; Blättler et al., 2011; Monteiro et al., 2012; Von Strandmann et al., 2013), and a combination of these changes coinciding with an increase in seasonality after a long eccentricity (2.4 Myr) cycle minimum (Mitchell et al., 2008; Batenburg et al., 2016).

The Cenomanian-Turonian interval is accompanied by exceptional warming of the ocean (Jenkyns et al., 1994; Clarke and Jenkyns, 1999; Bice et al., 2003; Voigt et al., 2004; Friedrich et al., 2012). Surface-ocean temperatures reached about 36°C at low latitudes (Forster et al., 2007; Moriya et al., 2007; MacLeod et al., 2013), and equator-to-pole sea surface temperature gradients were reduced to about 5°C (Huber et al., 2002; Linnert et al., 2014; O'Brien et al., 2017; Huber et al., 2018). Regionally, the warming during the OAE 2 interval is briefly interrupted by a cooling event known as the Plenus Cold Event that has been attributed to a decrease in atmospheric pCO_2 forced by the widespread burial of organic carbon (Kuypers et al., 1999; Voigt et al., 2006; Barclay et al., 2010; Sinninghe Damsté et al., 2010; Jarvis et al., 2011; van Bentum et al., 2012; Gale et al., 2019; O'Connor et al., 2020).

The Plenus Cold Event was first described in the Anglo-Paris Basin as the ingression of macrofossil boreal fauna (Gale and Christensen, 1996), including the belemnite species *Praeactinocamax plenus*, in the Plenus Marl of the English Chalk (Jefferies, 1963) and later found to coincide with two positive $\delta^{18}O$ shifts of bulk carbonates in the English section at Eastbourne (Jenkyns et al., 2017) as well as changes in Nd-isotope signatures (Zheng et al., 2013; O'Connor et al., 2020). Cooling in the early part of OAE 2 has been documented in other localities across the Tethyan margins, North Atlantic, and Western Interior Seaway based on faunal assemblages (Eicher and Diner, 1985; Leckie, 1985; Friedrich et al., 2006; Voigt et al., 2006; van Helmond et al., 2016; Eldrett et al., 2017), foraminiferal coiling direction (Desmares et al., 2016), $\delta^{18}O$ values (Keller et al., 2008; Kuhnt et al., 2017; Kalanat et al., 2018), and TEX_{86} measurements (Forster et al., 2007; Sinninghe Damsté et al., 2010). In the Western Interior Seaway, the Plenus Cold Event broadly coincides with an interval of increased abundance of benthic foraminifera suggesting extensive bottom water re-oxygenation that has been named the Benthonic Oxic Zone (Eicher and Worstell, 1970; Keller and Pardo, 2004; Prokoph et al., 2013; Eldrett et al., 2014).

Records of carbon burial and environmental changes during OAE 2 have been obtained mostly from sites in the low latitudes of the Atlantic Ocean, the Tethyan region, and the Western Interior Seaway (e.g. Tsikos et al., 2004; Bowman and Bralower, 2005; Kolonic et al., 2005; Caron et al., 2006; Sageman et al., 2006; Mort et al., 2007; Parente et al., 2008; Forster et al., 2008; Voigt et al., 2008; Takashima et al., 2009; Jarvis et al., 2011; van Bentum et al., 2012; Owens et al., 2013; Bomou et al., 2013; Du Vivier et al., 2014; Eldrett et al., 2014; Desmares et al., 2016; Robinson et al., 2017; Kuhnt et al., 2017; Grosheny et al., 2017; Heimhofer et al., 2018; Charbonnier et al., 2018; Gale et al., 2019, among many others). To date only few isolated records documenting the expression of OAE 2 from the southern high latitudes have been described (e.g., New Zealand: Hasegawa et al., 2013 and Gangl et al., 2019; Kerguelen Plateau: Dickson et al., 2017; Exmouth Plateau: Rullkötter et al., 1992 and Thurow et al., 1992; Cauvery Basin: Govindan and Ramesh, 1995). The relative lack of data from austral regions compromises efforts at global-scale interpretations of OAE 2.

OAE 2 environmental perturbations certainly influenced the evolutionary history of planktonic organisms (e.g., Erbacher et al., 1996; Leckie et al., 2002; Erba, 2004; Pearce et al., 2009). The planktonic foraminiferal record across OAE 2 at low latitudes is characterized by a significant turnover due to the extinction of the single-keeled rotaliporids (genera *Rotalipora* and *Thalmanninella*) and to the appearance and progressive diversification of double-keeled taxa (genera *Dicarinella* and *Marginotruncana*), genera that dominated planktonic foraminiferal assemblages until the Santonian (e.g., Robaszynski et al., 1990, 1993; Premoli Silva and Sliter, 1999; Leckie et al., 2002; Falzoni et al., 2016, 2018). Correlative records from across the Cenomanian/Turonian boundary and the OAE 2 interval at high latitudes in the Southern Hemisphere are poorly known. Planktonic foraminifera are reported from the Cauvery Basin in southeast India (Tewari et al., 1996) and from the Narmada Basin in northwest India (Keller et al., 2021), but this group is absent from studied New Zealand samples (Hasegawa et al., 2013) and is rare at Naturaliste Plateau (Herb, 1974) and Exmouth Plateau (Wonders, 1992), and in the southern Carnarvon Basin (Dixon et al., 2003; Haig et al., 2004). Until this study, the best high latitude record is from the Kerguelen Plateau (Ocean Drilling Program Site 1138), and although the OAE 2 is not complete, with a hiatus spanning

the onset of the event (Dickson et al., 2017), it contains a relatively well preserved planktonic foraminiferal assemblages characterized by low diversity and absence of Tethyan marker species (Petrizzo, 2001).

Sedimentary sequences recovered by IODP (International Ocean Discovery Program) Expedition 369 in the Mentelle Basin (Indian Ocean, SW Australia; Fig. 1), located at 60–62°S paleolatitude during the mid-Cretaceous (Hay et al., 1999; Müller et al., 2016; Scotese, 2016), are particularly intriguing since they provide high-resolution samples well suited for performing detailed studies of the organic-rich sediments occurring across the Cenomanian-Turonian boundary interval at high paleolatitudes in the Southern Hemisphere (Huber et al., 2019a). Moreover, the sediments recovered by IODP Expedition 369 at Sites U1513 and U1516 (Fig. 1) contain planktonic foraminifera and calcareous nannofossils with preservation sufficiently good to obtain biostratigraphic and paleoecological information enhancing our currently limited knowledge of the paleoceanographic perturbations during OAE 2 at southern high latitudes (Huber et al., 2019a). This study is focused on IODP Site U1516 with the aim of 1) providing a biochemostratigraphic framework that allows identification of the Cenomanian/Turonian boundary and OAE 2 at 60–62°S paleolatitude, and 2) examining the composition of the planktonic foraminiferal assemblages to interpret variations in the paleoceanographic patterns of the water column during OAE 2 and into the subsequent Turonian time interval.

2. Materials and methods

This study primarily focuses on samples across the Cenomanian-Turonian boundary interval from IODP Holes U1516C (34°20.9272′S, 112°47.9711′E) and U1516D (34°20.9277′S, 112°47.9573′E) drilled at 2676.6 m water depth in the south-central Mentelle Basin on the eastern flank of the Naturaliste Plateau in the Indian Ocean (SW Australia) (Fig. 1). Details on the drilling operations, logging, physical properties, magnetostratigraphy, geochemistry and sedimentology for Site U1516 are presented in the IODP Expedition 369 proceedings report (Huber et al., 2019a). Data from Holes U1516C (cores 26R to 35R) and U1516D (Fig. 2) are plotted in meters on the rCCSF depth scale (revised Core Composite Depth below Sea Floor, equivalent to mcd, meters composite depth), which is slightly revised from the shipboard splice (Huber et al., 2019a). A shipboard splice is constructed using colour data (RGB green) and XRF core-scanning data (Fe counts) and other data for overlapping portions of multiple holes drilled at the same site to suggest intervals

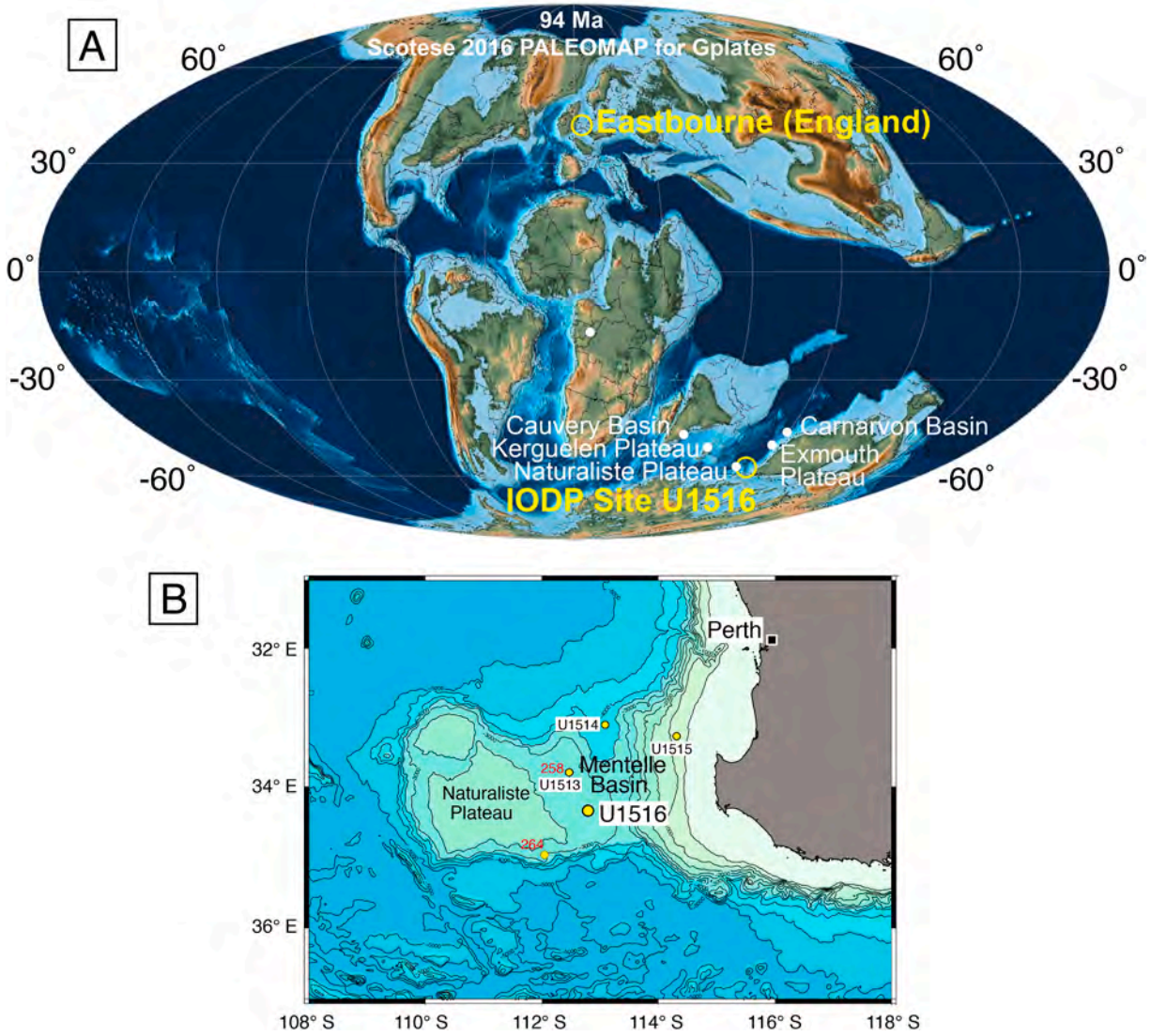

Fig. 1. A, Paleogeographic reconstruction for the late Cenomanian (94 Ma), with locations of IODP 369 Site U1516, and the Eastbourne section in England and other locations at southern high latitudes mentioned in the text (Scotese, 2016). B, Location of the sites drilled during IODP 369 and nearby DSDP Sites 258 and 264 (modified after Huber et al., 2019a).

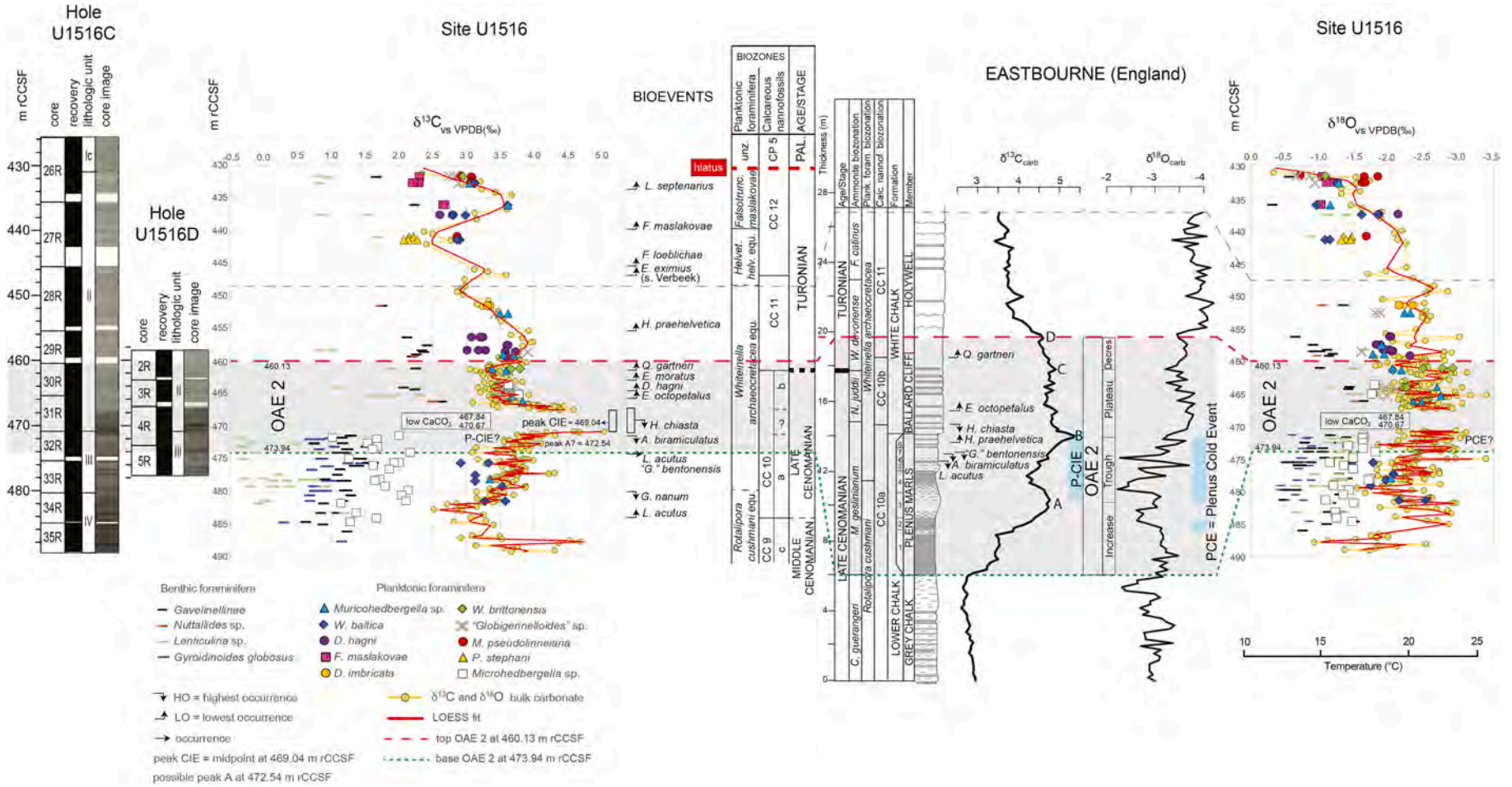

Fig. 2. Holes U1516C and U1516D: core recovery, lithologic units, core images and interval of low $CaCO_3$ content (467.84–470.67 m rCCSF) according to Huber et al. (2019a). $\delta^{13}C$ and $\delta^{18}O$ of bulk carbonate and foraminifera from this study. Planktonic foraminifera and calcareous nannofossil biostratigraphy from this study. The Cenomanian/Turonian boundary is approximated at the lowest occurrence of *Quadrum gartneri*. Hiatus between Turonian and Paleocene according to Huber et al. (2019a) and this study. OAE 2 (Oceanic Anoxic Event 2) is identified following Jarvis et al. (2011), Gambacorta et al. (2015) and Jenkyns et al. (2017) as the interval from the base of the beginning of the positive excursion in $\delta^{13}C$ to the point at the first highest $\delta^{13}C$ value on the decline of the $\delta^{13}C$ values to pre-excursion values (gray band). The peak CIE is placed at the midpoint between the two highest $\delta^{13}C$ values above and below the interval of low $CaCO_3$ content. The P-CIE (Plenus Carbon Isotope Excursion, O'Connor et al., 2020) may correspond to the interval of a negative $\delta^{13}C$ excursion coinciding with the trough in the $\delta^{13}C$ profile. The Plenus Cold Event (PCE) should coincide with the highest $\delta^{18}O$ carbonate bulk values by comparison with Eastbourne (e.g., Jenkyns et al., 2017). m rCCSF = revised Core Composite depth below Sea Floor in meters. Eastbourne section (England): lithostratigraphy, $\delta^{13}C_{carb}$ $\delta^{18}C_{carb}$ after Tsikos et al. (2004) and Pearce et al. (2009). Planktonic foraminiferal biostratigraphy and bioevents after Falzoni et al. (2018). Calcareous nannofossil biostratigraphy and bioevents after Paul et al. (1999), Tsikos et al. (2004) and Linnert et al. (2011) using the biozonations by Sissingh (1977) and Perch-Nielsen (1985). Age/stage and ammonite biostratigraphy after Gale et al. (2005). Peaks A to D on the carbon isotope curve according to previous authors (e.g., Jarvis et al., 2006; Voigt et al., 2008; O'Connor et al., 2020). OAE 2 interval and Plenus Cold Event (PCE) according to Jenkyns et al. (2017). P-CIE according to O'Connor et al. (2020).

least disturbed by coring and best suited for study of temporal trends (Huber et al., 2019b; LIMS online report portal at http://web.iodp.tamu.edu/LORE/).

The Cretaceous sedimentary sequence in Hole U1516C starts in core 26R-4, 105 cm at 431.56 m rCCSF with Turonian sediments overlain by an unconformity that separates the Cretaceous sediments below from Paleocene sediments above (lithostratigraphic Unit Ic, Fig. 2). The unconformity is defined by sharp changes in the foraminiferal and nannofossil assemblages and a decrease in NGR (Natural Gamma Radiation) and magnetic susceptibility (Huber et al., 2019a). The lithologies from core 26R-4, 105 cm to core 31R-4, 119 cm in Hole U1516C and from core 2R to core 4R-3, 31 cm in Hole U1516D are assigned to lithostratigraphic Unit II (Fig. 2) and are composed of white, light olive brown, and light gray calcareous chalk interbedded with chert that grades gradually downsection into light greenish gray and greenish gray calcareous/nannofossil chalk with clay interbedded with chert and claystone. From core 31R-4 to core 33R-CC in Hole U1516C and from core 4R-3 to core 5R-CC in Hole U1516D the lithologies are assigned to lithostratigraphic Unit III (Fig. 2) and consist of an alternating sequence of black, light greenish gray, greenish gray, and very dark greenish gray claystone (sometimes with common to abundant nannofossils) and clayey nannofossil chalk. Cores 34R and 35R in Hole U1516C are assigned to lithostratigraphic Unit IV, which is composed of a sequence of massive to mottled black and dark greenish gray nannofossil-rich claystone and claystone with nannofossils (Huber et al., 2019a).

For microfossil analysis rock samples were dried, weighed and soaked in a solution of tap water and H_2O_2, washed over 250, 125 and 38 μm sieves and dried to obtain washed residues. For each size fraction microfossil groups and planktonic foraminifera genera and species were counted in splits of the washed residues large enough to be statistically reliable. The number of specimens for each category were multiplied by the number of splits and the total number of specimens were obtained for each sample by adding the values of the three size fractions. Absolute abundances of foraminifera and radiolaria were calculated as the number of specimens per gram of dry sediment. Planktonic foraminiferal taxonomy follows the pforams@mikrotax database (Huber et al., 2016). The planispiral genus *Globigerinelloides* is placed in quotes in the text and figures because it is polyphyletic and currently under taxonomic revision (see discussion in Petrizzo et al., 2017). The planktonic foraminiferal biozonation follows Robaszynski and Caron (1995), Petrizzo (2003) and Petrizzo et al. (2020).

Samples for calcareous nannofossils were prepared following the double slurry method of Watkins and Bergen (2003). At least 400 fields of view were examined from each sample that was not barren of calcareous nannofossils. The taxonomy for calcareous nannofossils largely follows that of Nannotax3 (mikrotax.org/Nannotax3); however, the definition of *Eiffellithus eximius* sensu Verbeek follows that in Huber et al. (2017) and Gaer and Watkins (2020). The biozonation for calcareous nannofossils is according to Perch-Nielsen (1985) and Huber et al. (2017) and age assignments follow Gradstein et al. (2012).

Stable isotope values for foraminifera and bulk carbonate were measured at the University of Missouri or in the Laboratory of Earth Environmental Evolution at Kanazawa University. Foraminiferal data was obtained from single species separates of well-preserved planktonic and benthic foraminifera picked from samples where sufficient number of such individuals were present. Most samples from Hole U1516C core 28R are weakly indurated and yielded foraminifera that are both strongly recrystallized and infilled with sparry calcite so were not analyzed. Bulk samples measured at the University of Missouri were milled from chips under a 3× magnifying lens using an engraving tool operated at low speed whereas at Kanazawa University a portion of each bulk sample was powdered using a mortar and pestle.

Foraminiferal tests (shells) and a subset of the bulk carbonate samples were measured on Kiel III carbonate device operated at 70°C and Delta Plus IRMS at the University of Missouri. Measurement error is +/− 0.04‰ and +/− 0.06‰ (1 standard deviation) for $\delta^{13}C$ and $\delta^{18}O$ respectively based on uncorrected, replicate analyses of NBS-19 run throughout the duration of the study. Sample values were corrected to nominal values of 1.95‰ ($\delta^{13}C$) and − 2.20‰ ($\delta^{18}O$) for the average of NBS-19 analyses within each run.

Bulk samples analyzed at Kanazawa University were dried overnight, then a split was weighed (ca. 0.3 mg each) with a Sartorius MC5 microbalance for analysis. Carbon dioxide was produced by reaction with 100% phosphoric acid in helium atmosphere at 70°C through GasBenchII (ThermoFisher), and the gas was introduced and analyzed by a Delta V Advantage (ThermoFisher) mass spectrometer. The reference NBS19 ($\delta^{18}O$: −2.20‰; $\delta^{13}C$: +1.95‰) was analyzed twice daily and used for international calibration. Laboratory standard carbonates were analyzed more often to check the stability of the machine. Analytical errors of the isotopic measurement were less than 0.1‰ for both oxygen and carbon isotopes during the analyses of all samples studied.

All stable isotopic data are reported on the Vienna-PDB scale. Paleotemperatures derived from planktonic and benthic foraminifera $\delta^{18}O$ were calculated using the equations and assumptions detailed in Huber et al. (2018). The bulk carbonate and foraminifera stable isotope data are reported in Supplementary Data Tables 1 and 2.

3. Carbon and oxygen isotope data for bulk carbonate

Bulk carbonate results (382 analyses from 273 samples; Supplementary Data Table 1) show trends in surface water values with highest sampling density from 459 to 486 m rCCSF (Fig. 2). Replicate analyses demonstrate generally excellent reproducibility within samples and between labs as well as coherent stratigraphic trends (Fig. 2; Supplementary Data Table 1). Analyses on 9 samples from 467.49–470.62 m rCCSF failed to yield meaningful data due to the low-carbonate content of these samples, and 11 analyses (from 5 samples) had $\delta^{13}C$ values <2‰. These latter results are the lowest 11 $\delta^{13}C$ values measured among the bulk samples and 3 of the samples had relatively low carbonate content. Anomalously low $\delta^{13}C$ values (relative to the rest of the data set) can be explained by contributions from benthic bioclasts, presence of diagenetic carbonate with a significant contribution from reminerализed organic carbon, and/or analytical error in the powders analyzed. Although $\delta^{18}O$ values in these samples do not seem similarly anomalous, the 11 measurements are excluded from the plots but are included in the data file (Supplementary Data Table 1).

Values plotted represent replicate averages for each sample (Fig. 2). In addition to trends on the meter-scale, considerable variation much larger than analytical error is present on shorter length scales. This variability likely reflects a combination of short-term changes in surface water conditions, changes in the nannofossil assemblages that are assumed to represent the dominant component of the bulk carbonate in any sample, and sampling biases (e.g., contributions from other bioclasts in the powder analyzed). Lithologic variation suggest short-term oceanographic variations are likely. For example, the 4 relatively low $\delta^{13}C$ values spaced ~1 m apart between 473 and 476 m rCCSF (Fig. 2) are all from relatively dark lithologies; however, the spacing of darker lithologies in this interval is ~30 cm. Thus, those 4 $\delta^{13}C$ minima may represent an aliasing of higher frequency cyclic alternations that are not accurately captured with our sampling resolution. To reduce the influence of such factors which are beyond the scope of this study, meter scale trends in the bulk carbonate data are highlighted with trendlines (Fig. 2). The trendlines were generated using the LOESS function in Matlab, with a window of 3 (i.e., a series of quadratic polynomial fits spanning 7 data points weighted by proximity to the point of interest). The window was chosen to smooth across high-resolution variability in the interval of highest sampling density without overly dampening differences among samples separated by meters in the intervals with lower sampling density (Fig. 2).

4. Integrated biostratigraphy

The calcareous plankton assemblages at Site U1516 are characterized by the absence of several taxa that are normally common at mid- to low latitudes, including most of the marker taxa used to constrain the Cenomanian-Turonian boundary interval. Nevertheless, the record at Site U1516 can be correlated with records at low latitudes in the Tethys (e.g., Eastbourne, England and Tarfaya, Morocco: Tsikos et al., 2004) and Western Interior Seaway (e.g., Pueblo, Colorado: Tsikos et al., 2004; Caron et al., 2006) using the calcareous plankton bioevents combined with the carbon isotopic data (Table 1; Fig. 2). Together, these results provide a good chronostratigraphic framework and integrated stratigraphy that represents one of the best documented record across the Cenomanian-Turonian boundary interval for high latitudes of the Southern Hemisphere.

The base of the studied stratigraphic interval in Hole U1516C, core 35R (484.29 m rCCSF to 489.58 m rCCSF) lacks calcareous plankton marker events because of poor preservation and a low number of taxa. Nevertheless, it is assigned to the early Cenomanian CC 9c Zone based on the calcareous nannofossil assemblages. The first sample (U1516C-34R-4, 6–8 cm at 484.29 m rCCSF) yielding a rich calcareous nannofossil assemblages contains the calcareous nannofossil *Lithraphidites acutus* whose lowest occurrence (LO) identifies the base of the CC 10a Zone. This appearance level is probably delayed at Site U1516 because of poor preservation of the nannofossil assemblages in the underlying interval. The highest occurrence (HO) of *Gartnerago nanum* is recorded in sample U1516C-33R-CC, 1–5 cm at 480.07 m rCCSF. The concurrent range of L. *acutus* and *G. nanum* in core U1516C-34R, indicates the lower part of CC 10a Zone corresponding to a middle to early-late Cenomanian age (Gradstein et al., 2012) and was reported from stratigraphic intervals that encompass the Mid-Cenomanian Event at some localities (Demerara Rise, central Atlantic Ocean: Hardas et al., 2012; Newfoundland Basin: Urquhart et al., 2007).

The highest occurrences of *Helenea chiasta* at 470.89 m rCCSF allows identification of the base of the early Cenomanian CC 10b Zone (Fig. 2). At Site U1516 it is preceded by the HO of *Axopodorhabdus biramiculatus* (= *Axopodorhabdus albianus* of some authors) at 471.48 m rCCSF and these bioevents are documented to bracket the interval with the highest $\delta^{13}C$ values within the OAE 2 Carbon Isotope Excursion (CIE) at Eastbourne in England (Paul et al., 1999; Linnert et al., 2011), at Clot Chevalier in France (Gale et al., 2019), in Tunisia (Nederbragt and Fiorentino, 1999), and in the Western Interior Seaway (Corbett et al., 2014). Moreover, the HO of *H. chiasta* is registered immediately below the interval of low carbonate content ($CaCO_3$ = 0.02–0.69 wt%, from 467.84 to 470.67 m rCCSF; Huber et al., 2019a) suggesting that its distribution may be truncated at Site U1516 (Fig. 2).

The planktonic foraminifera *"Globigerinelloides" bentonensis* is a very reliable marker species in the latest Cenomanian at low latitudes where it last occurs in the upper part of calcareous nannofossil CC 10a Zone at a level close to the extinction of *Rotalipora cushmani* (Pueblo, Colorado: Leckie, 1985; Eicher and Diner, 1985; Keller and Pardo, 2004. Eastbourne, England: Paul et al., 1999; Keller et al., 2001; Falzoni et al., 2018. Clot Chevalier, France: Falzoni et al., 2016; Gale et al., 2019. Ganuza, Spain: Lamolda et al., 1997. Tarfaya, Morocco: Keller et al., 2008; Falzoni et al., 2018). At Site U1516 the highest occurrence of *"G." bentonensis* is recorded at 474.11 m rCCSF close to the HO of *L. acutus* at 474.12 rCCSF (Table 1; Fig. 2). Both taxa are rare and show sporadic occurrences at Site U1516, and, consequently, their disappearance levels are interpreted to be diachronous and not reliable for correlation.

The Cenomanian/Turonian boundary is formally defined by the lowest occurrence of the ammonite *Watinoceras devonense* in the GSSP section at Pueblo, Colorado (Kennedy et al., 2000, 2005). In the absence of this primary criterion the boundary at Site U1516 is placed at the LO of the calcareous nannofossil *Quadrum gartneri* (at 461.68 m rCCSF) (Fig. 2). The LO of *Quadrum gartneri* marks the base of CC 11 Zone and is a consistently reliable datum for approximating the base of the Turonian Stage, as it occurs slightly above the stage criterion in the GSSP type section as well as in many other localities worldwide (e.g., Tsikos et al., 2004; Linnert et al., 2010, 2011; Gradstein et al., 2012; Corbett et al., 2014; Dickson et al., 2017; Gale et al., 2019).

The planktonic foraminifera *Rotalipora cushmani* and *Helvetoglobotruncana helvetica* whose HO and LO, respectively, are used to constrain and approximate the Cenomanian/Turonian boundary at low to mid-latitudes (e.g., Paul et al., 1999; Keller et al., 2001; Kennedy et al., 2000, 2005; Caron et al., 2006; Desmares et al., 2007; Gradstein et al., 2012; Elderbak and Leckie, 2016; Falzoni et al., 2016, 2018; Falzoni and Petrizzo, 2020) are absent from the Mentelle Basin. At Site U1516 the planktonic foraminifera *Helvetoglobotruncana praehelvetica*, which is ancestral to *H. helvetica* (e.g., Hart and Weaver, 1977; Hart and Leary, 1989; Huber and Petrizzo, 2014), first occurs at 455.25 m rCCSF, above the LO of *Q. gartneri* in the lower Turonian (Table 1; Fig. 2). An early Turonian LO is in disagreement with *H. praehelvetica*'s distribution at low latitudes where its LO is recorded in the late Cenomanian either in the upper *R. cushmani* Zone (Pueblo, Colorado: Leckie, 1985. Umbria-Marche Basin, Italy: Premoli Silva and Sliter, 1995; Mort et al., 2007. Dolomites, Italy: Luciani and Cobianchi, 1999. North Atlantic: Huber

Table 1
Planktonic foraminifera, calcareous nannofossil bioevents, and peak and base of the Carbon Isotope Excursion (CIE) at Site U1516. *Axopodorhabdus biramiculatus* = *Axopodorhabdus albianus* of some authors. FAD = first appearance datum; LAD = last appearance datum; LO = lowest occurrence; HO highest occurrence. Age of the bioevents according to Gradstein et al. (2012). Ages of peak CIE and base CIE according to Joo and Sageman (2014) and Joo et al. (2020). nd = no data available. nt = bioevent not reliable at Site U1516, see text for explanation. Top and bottom revised Core Composite depth below Sea Floor (rCCSF) in meters. Plotcode in the depth-age model shown in Fig. 4.

Event	Sample TOP	TOP m rCCSF	Sample BOTTOM	BOTTOM m rCCSF	Age (Ma)	Plotcode
FAD *Lithastrinus septenarius*	U1516C-26R-6, 89–90 cm	434.16	U1516C-27R-1, 7–10 cm	436.07	91.78	bLs
LO *Falsotruncana maslakovae*	U1516C-27R-3, 117–120 cm	440.04	U1516C-27R-4, 58–61 cm	440.96	nd	
FAD *Eiffellitus eximius* (s. Verbeek)	U1516C-28R-1, 110–113 cm	446.70	U1516C-28R-3, 105–108 cm	449.33	92.99	bEe
LO *Falsotruncana loeblichae*	U1516C-28R-1, 10–13 cm	445.70	U1516C-28R-3, 65–68 cm	446.25	nd	
LO *Helvetoglobotruncana praehelvetica*	U1516C-29R-1, 5–8 cm	455.25	U1516C-29R-1, 120–123 cm	456.40	nt	
FAD *Quadrum gartneri*	U1516C-30R-2, 95–96 cm	461.68	U1516C-30R-2, 134–137 cm	462.06	93.55	bQg
FAD *Eprolithus moratus*	U1516C-30R-3, 71–75 cm	462.92	U1516C-30R-3, 131–133 cm	463.48	93.73	bEm
LO *Dicarinella hagni*	U1516D-3R-1, 121–123 cm	464.14	U1516D-3R-2, 15–18 cm	464.39	nt	
FAD *Eprolithus octopetalus*	U1516C-31R-2, 8–11 cm	465.79	U1516C-31R-2, 97–100 cm	466.68	93.80	bEo
LAD *Helenea chiasta*	U1516C-31R-2, 8–11 cm	465.79	U1516C-32R-1, 97–100 cm	470.89	93.90	tHc
peak CIE	U1516C-31R-3, 38–39 cm	467.37	U1516C-32R-1, 80–82 cm	470.72	94.17	pCIE
LAD *Axopodorhabdus biramiculatus*	U1516C-32R-1, 131–134 cm	471.24	U1516C-32R-2, 4–7 cm	471.48	94.20	tAb
HO *Lithraphidites acutus*	U1516C-32R-3, 111–113 cm	474.05	U1516C-32R-CC, 1–5 cm	474.12	nt	tLa
HO *"Globigerinelloides" bentonensis*	U1516C-32R-3, 111–113 cm	474.05	U1516C-32R-CC, 0–5 cm	474.11	nt	tGb
base CIE	U1516C-32R-3, 100–101 cm	473.94	U1516C-32R-3, 100–101 cm	473.94	94.59	bCIE
LAD *Gartnerago nanum*	U1516C-33R-5, 3–7 cm	479.29	U1516C-33R-CC, 1–5 cm	480.07	94.79	tGn
FAD *Lithraphidites acutus*	U1516C-34R-4, 6–8 cm	484.29	U1516C-35R-1, 87–90 cm	485.76	96.16	bLa

et al., 1999. Eastbourne, England: Falzoni et al., 2018) or in the lower *Whiteinella archaeocretacea* Zone (Kaalat Senan, central Tunisia: Robaszynski et al., 1990. Ganuza, northern Spain: Lamolda et al., 1997). The variable position of *H. praehelvetica*'s LO renders this an unreliable marker for cross-latitude correlation (Falzoni et al., 2018).

Similarly, the LO of *Dicarinella hagni* is recorded within the *R. cushmani* Zone and calcareous nannofossil CC 10a Zone at Eastbourne and in other low latitude sections (Falzoni et al., 2018), whereas its appearance level is delayed at Site U1516, falling above the HO of *H. chiasta* at 464.14 m rCCSF within calcareous nannofossil CC 10b Zone. Because of the absence of the biozonal markers (*R. cushmani* and *H. helvetica*) and the diachroneity of planktonic foraminiferal events that are present, planktonic foraminiferal biozones from the base of the studied section to core 27R in Hole U1516C (Fig. 2) are identified according to their stratigraphic positions and equivalence with the low latitude biozones (*Rotalipora cushmani* Zone, *Whiteinella archaeocretacea* Zone and *Helvetoglobotruncana helvetica* Zone: Robaszynski and Caron, 1995; Premoli Silva and Sliter, 1995) as constrained by correlation with the calcareous nannofossil events.

The LO of *Eiffellitus eximius* at 446.70 m rCCSF and LO of *Falsotruncana maslakovae* at 440.04 m rCCSF allow identification of the base of the calcareous nannofossil CC 12 Zone and the base of the planktonic foraminifera *Falsotruncana maslakovae* Zone (Petrizzo et al., 2020) in the late Turonian (Fig. 2) in agreement with data from Tanzania at 35°S paleolatitude and from the Exmouth Plateau at 47°S paleolatitude (Huber et al., 2017).

Correlation of the bioevents of Site U1516 to the biostratigraphically well-characterized and stratigraphically expanded section of semi-lithified chalk exposed at Eastbourne, England (e.g., Paul et al., 1999; Tsikos et al., 2004; Linnert et al., 2011) provides evidence of the correlation accuracy and precision of the biostratigraphic events occurring at both localities (Fig. 2). A graphic correlation and calculation of the correlation coefficient of the best-fit regression line is applied (e.g., Shaw, 1964; Hart and Leary, 1991; Sadler, 2004; Paul and Lamolda, 2009; Petrizzo et al., 2011, Petrizzo et al., 2017; Smith et al., 2015; Huber et al., 2017; Olayiwola et al., 2017; Falzoni et al., 2018; Petrizzo, 2019). The best-fit regression line from a cross-plot using the shared bioevents and the position of the maximum Carbon Isotope Excursion (= peak CIE at Site U1516 estimated at the midpoint of the interval of low carbonate content and peak B at Eastbourne; Figs. 2 and 3) in the two sections provides a correlation coefficient of 0.99 (Fig. 3), which supports the reliability of the sequence of microfossil index species and of the stratigraphic correlation between Site U1516 and the Eastbourne section (Fig. 2).

5. Identification of OAE 2 and the Plenus Cold Event

The bulk carbon isotope record at Site U1516 shows a sharp positive $\delta^{13}C$ excursion of 1.5‰ from 465.47 to 473.94 m rCCSF which brackets an interval (from 467.84 to 470.67 m rCCSF) that registers the lowest $CaCO_3$ values (0.02–0.69 wt%) and contains the highest TOC (Total Organic Carbon) value of 14.59 wt% at 469.95 m rCCSF (sample U1516C-32R-1, 1–2 cm; Huber et al., 2019a) within the interval studied (Fig. 2). Correlation of the $\delta^{13}C$ profile of Site U1516 to the Eastbourne section (Tsikos et al., 2004) underscores the complexity of details of the $\delta^{13}C$ record in both regions (Fig. 2). General features of the $\delta^{13}C$ curve of the Eastbourne section and of other sections spanning the Cenomanian-Turonian boundary interval (e.g., Pueblo, Colorado: Pratt and Threlkeld, 1984; Pratt, 1985; Caron et al., 2006. Pont d'Issole, Vocontian Basin: Jarvis et al., 2011. Clot Chevalier, Vocontian Basin: Gale et al., 2019. Tibet: Wendler, 2013) include a relatively sharp initial increase, a first peak, a trough, a second peak, and a plateau followed by a gradual decrease to pre-excursion values (Fig. 2).

The OAE 2 interval is identified from the level of the initial positive shift into the $\delta^{13}C$ excursion (onset) through the level where $\delta^{13}C$ values begin a definite decrease from those high values (termination) (e.g., Jarvis et al., 2011; Gambacorta et al., 2015; Jenkyns et al., 2017). The main features of the $\delta^{13}C$ curve documented at Site U1516 match

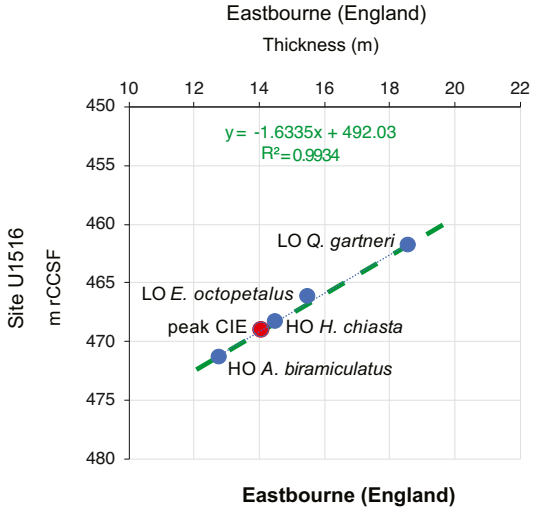

Eastbourne (England) **Site U1516**

Bioevents	Thickness (m)	References	midpoint m rCCSF	References
LO *Quadrum gartneri*	18.6	Tsikos et al., 2004	461.87	This study
LO *Eprolithus octopetalus*	15.7	Linnert et al., 2011	466.23	This study
HO *Helenea chiasta*	14.5	Paul et al., 1999	468.34	This study
peak CIE = peak B	14.1	Jarvis et al., 2006	469.04	This study
HO *Axopodorhabdus biramiculatus*	12.8	Tsikos et al., 2004	471.36	This study

Fig. 3. Graphic correlation of the common biostratigraphic events and the position of the maximum Carbon Isotope Excursion between Site U1516 (peak CIE) and the Eastbourne section (peak B). The best-fit regression line is shown in green. *Axopodorhabdus biramiculatus* = *Axopodorhabdus albianus* of some authors. Blue circles = calcareous nannofossils; red circle = peak CIE; m rCCSF= revised Core Composite depth below Sea Floor in meters.

features at Eastbourne allowing placement of the base of the OAE 2 CIE at 473.94 m rCCSF coinciding with the beginning of the positive $\delta^{13}C$ excursion, and of the top of OAE 2 at the first highest $\delta^{13}C$ value in the decline of the $\delta^{13}C$ values at 460.13 m rCCSF, which corresponds to peak D at Eastbourne and is above the LO of *Q. gartneri* (Fig. 2).

The age-depth plot for Site U1516 (Fig. 4) is build using calcareous nannofossil and planktonic foraminifera bioevent ages and the ages for the base and peak CIE (Table 1). Determination of a best-fit line of correlation (LOC) provides a means for interpreting the sedimentation rates at Site U1516. The LOC, drawn through the bioevents that are deemed to be most reliable and the peak and base CIE, highlights a marked decrease in sedimentation rates within OAE 2 which is consistent with the low $CaCO_3$ content from 467.84 to 470.67 m rCCSF (Fig. 4). According to the age-depth model and to the calculated sedimentation rates at Site U1516, the duration of the OAE 2 interval is estimated as ~0.9 m.y (Fig. 4), which is similar to the duration determined previously for stratigraphic sections located at high latitudes of the Southern Hemisphere (New Zealand at 70° paleolatitude: Gangl et al., 2019).

The Plenus Cold Event, a cold snap locally interrupting the hot greenhouse phase within OAE 2 (e.g., Voigt et al., 2006; Sinninghe Damsté et al., 2010; Jarvis et al., 2011; Jenkyns et al., 2017; Gale et al., 2019) is identified in the Eastbourne section by the southward invasion of cool-water boreal fauna into lower latitudes (Gale and Christensen, 1996). At Eastbourne the correlation between the stratigraphic distribution of the cool-water fauna and positive oxygen isotope values suggest that the Plenus Cold Event was actually characterized by two cooling intervals separated by a warmer episode (Jenkyns et al., 2017) of which the stratigraphically upper cooler interval coincides with the position of a trough in the $\delta^{13}C$ curve (Fig. 2). The presence of a temporary negative $\delta^{13}C$ shift superimposed on the overall positive $\delta^{13}C$ excursion during OAE 2 is registered in numerous Northern Hemisphere sections (e.g., Tsikos et al., 2004; Kuhnt et al., 2005; Sageman et al., 2006; Hasegawa et al., 2010; Jarvis et al., 2011; Jenkyns et al., 2017), in few localities in the Southern Hemisphere (New Zealand: Hasegawa et al., 2013; Gangl et al., 2019). According to O'Connor et al. (2020) the negative carbon-isotope excursion (P-CIE) during the Plenus Cold Event interval was a global event coinciding with a CO_2 increase; however, the negative $\delta^{13}C$ shift is difficult to trace at Site U1516. If resolvable at Site U1516, it could be correlated with a trough within the positive $\delta^{13}C$ excursion in the interval from 470.72 to 472.54 m rCCSF where the $\delta^{13}C$ values are 0.5–1.0‰ lower than peak values (Fig. 2).

The bulk carbonate $\delta^{18}O$ record at Site U1516 through OAE 2 exhibits an overall decreasing trend punctuated by transient episodes of high $\delta^{18}O$ values (Fig. 2). Lowest values (suggesting peak warmth) are reached from above the interval with low $CaCO_3$ content and peak $\delta^{13}C$ values (from 464.67 to 470.72 m rCCSF), suggesting that highest sea surface temperatures in the Mentelle Basin occurred during or just after the strongest environmental perturbation. The $\delta^{18}O$ bulk carbonate record within the OAE 2 interval is characterized by strong fluctuations of the $\delta^{18}O$ values varying from −1.69 to −3.46‰ with the highest values near the base of OAE 2 in the stratigraphic interval from 470.72 to 472.54 m rCCSF, which could be time-equivalent to the Plenus Cold Event at Eastbourne (Fig. 2).

6. Composition of the microfossil assemblages

The planktonic foraminiferal assemblages at Site U1516 are characterized by dominance of small-sized specimens (125–38 μm) throughout and by low absolute abundances of large-sized taxa (> 125 μm), which are only sporadically present in the late Cenomanian, and, while common in the Turonian, are still subordinate to small-sized specimens (Fig. 5). Preservation in the Cenomanian interval is generally good as most tests show no infilling and have only little evidence of secondary alteration. In the Turonian preservation ranges from good to moderate as tests exhibit small scale recrystallization. Several samples from core U1516C-28R yield foraminifera that are strongly recrystallized and infilled with sparry calcite.

The patterns of absolute abundances among benthic foraminifera parallels the planktonic foraminifera, although planktonic foraminifera generally have about twice or more the absolute abundance of benthic foraminifera. At Site U1516 radiolaria (Erbacher, 2021), mainly belonging to the order Nassellaria, show a marked increase in abundance in the late Cenomanian with the larger specimens more abundant in the interval of low $CaCO_3$ content, while they are only sporadically present in the Turonian (Fig. 5).

The interval below OAE 2 (from 474.02 to 489.42 m rCCSF) is characterized by the presence of small sized planktonic and benthic foraminifera that display cyclic fluctuations and by the dominance of benthic foraminifera in the lowermost part of the studied sequence. Planktonic and benthic foraminifera still display cyclic fluctuations in the lower part of OAE 2 as mirrored by the Planktonic/Benthic ratio (Fig. 5). The stratigraphic interval within OAE 2 and coinciding with the interval of low $CaCO_3$ content, is characterized by the absence of

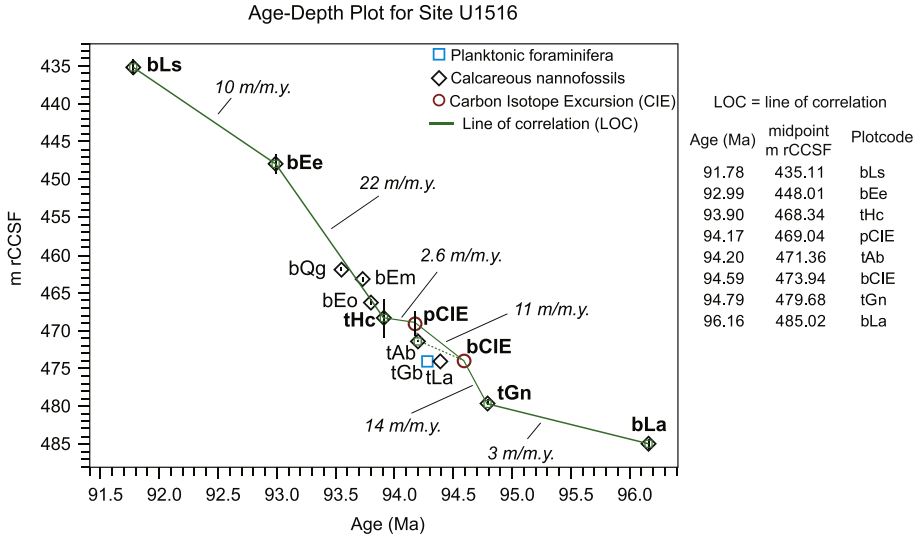

Fig. 4. Age-depth model based on calcareous nannofossils, planktonic foraminifera datums and the ages of the peak and base CIE showing the line of correlation (LOC) and the sedimentation rates in m/m.y. at Site U1516. See Table 1 for ages references of bioevents, peak and base CIE, and plotcode. m rCCSF= revised Core Composite depth below Sea Floor in meters.

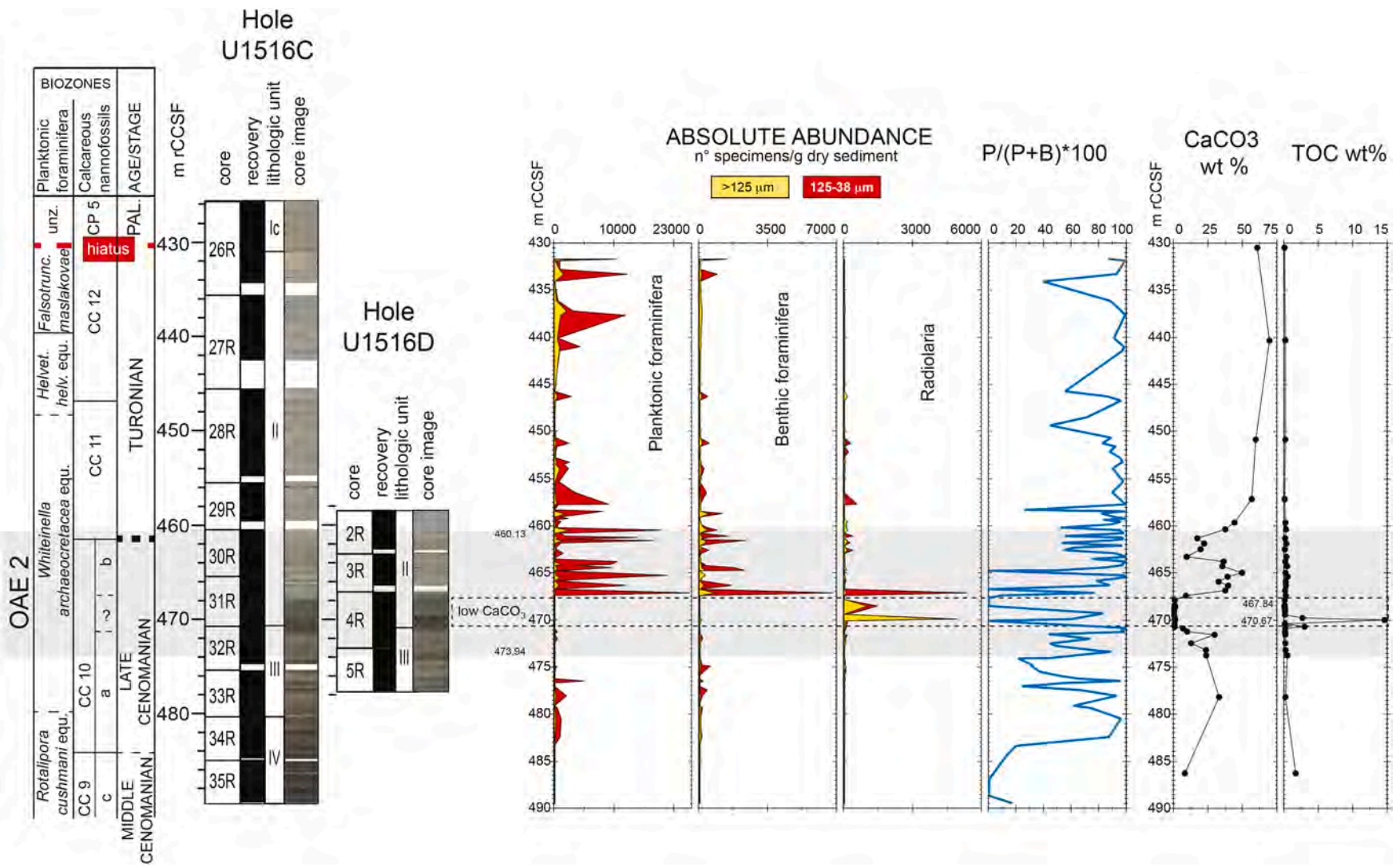

Fig. 5. Absolute abundance of planktonic foraminifera, benthic foraminifera and radiolaria, and planktonic/benthic ratio in Holes U1516C and U1516D. Core recovery, lithologic units, core images, $CaCO_3$ and TOC according to Huber et al. (2019a). Planktonic foraminifera and calcareous nannofossil biostratigraphy from this study. The Cenomanian/Turonian boundary is approximated at the lowest occurrence of *Quadrum gartneri*. OAE 2 (gray band) is identified following Jarvis et al. (2011) Gambacorta et al. (2015) and Jenkyns et al. (2017). m rCCSF = revised Core Composite depth below Sea Floor in meters. See text for further explanation.

foraminifera, except for three samples (from 469.26 to 469.87 m rCCSF) where some planktonic and benthic foraminifera are observed (Supplementary Data Table 3), and by the highest abundance of large and small-sized radiolaria (from 467.08 to 470.88 m rCCSF, cores U1516C-31R and U1516D-4R). This interval also coincides with the lowest $CaCO_3$ values (0.02–0.69 wt%) from 467.84 to 470.67 m rCCSF and the highest TOC value of 14.59 wt% at 469.95 m rCCSF (Huber et al., 2019a) (Fig. 5).

The absolute abundances of the small-sized planktonic and benthic foraminifera markedly increase in the upper part of OAE 2 reaching about 23,000 specimens/g dry sediment (cores U1516C-31R and U1516D-3R), which are the highest values observed at Site U1516 (Fig. 5).

Planktonic foraminifera from above OAE 2 to the top of the studied interval (sample U1516C-26R-4, 112–115 cm; 431.63 m rCCSF), immediately below the unconformity between the Cretaceous and Paleocene sediments at 431.56 m rCCSF, show fluctuations in absolute abundances varying from about 9,000 to 13,000 specimens/g of dry sediment with peak values in certain intervals in the upper part (cores U1516C-26R and 27R) of the Turonian record (Fig. 5).

7. Planktonic foraminiferal assemblages and absolute abundances

The composition of the planktonic foraminiferal assemblages at Site U1516 is characterized by low species diversity and the absence of the typical Cenomanian keeled genera (*Rotalipora*, *Thalmanninella*) while the other keeled genera (*Dicarinella*, *Marginotruncana*, *Praeglobotruncana*) occur with few species compared to the assemblages of equivalent age at mid-low latitudes in different paleogeographic and paleoceanographic settings (e.g., Western Interior Seaway: Eicher and Worstell, 1970; Eicher and Diner, 1985; Leckie, 1985; Leckie et al., 1998; Keller and Pardo, 2004; Caron et al., 2006; Desmares et al., 2007; Elderbak and Leckie, 2016; Lowery and Leckie, 2017. Eastbourne, England: Paul et al., 1999; Keller et al., 2001; Hart et al., 2002; Falzoni et al., 2018; Falzoni and Petrizzo, 2020. Tarfaya, Morocco: Keller et al., 2008; Falzoni et al., 2018. Vocontian Basin: Grosheny et al., 2006; Grosheny et al., 2017; Falzoni et al., 2016. Tunisia: Robaszynski et al., 1990, 1993; Caron et al., 2006; Nederbragt and Fiorentino, 1999. Blake Nose, NW Atlantic Ocean: Huber et al., 1999. Austria: Gebhardt et al., 2010. Switzerland: Strasser et al., 2001; Westermann et al., 2010. Spain: Lamolda et al., 1997. Umbria-Marche Basin, Italy: Premoli Silva and Sliter, 1995; Mort et al., 2007; Coccioni and Premoli Silva, 2015. Dolomites, Venetian Prealps and Sicily, Italy: Luciani and Cobianchi, 1999; Scopelliti et al., 2004; Coccioni and Luciani, 2005. Japan: Hasegawa, 1999. Tibet: Bomou et al., 2013).

Nevertheless, the detailed analysis of the specimens in the large-sized (> 125 μm) and small-sized fractions (125–38 μm) has permitted identification of a number of taxa (Supplementary Data Table 3) that improve our understanding of the stratigraphic distribution of planktonic foraminifera at southern high latitudes. At Site U1516 the late Cenomanian planktonic foraminiferal record is characterized by low diversity of genera and species, the latter ranging from 0 to 8. *Muricohedbergella* and the small-sized *Microhedbergella* and *"Globigerinelloides"* are the most common taxa throughout (Fig. 6). These genera are the only taxa occurring below and in the lower part of OAE 2 (below the interval of low $CaCO_3$ content). They reach their highest abundances (more than 20,000 specimens/g of dry sediment) within the middle part of OAE 2 immediately above the interval of low $CaCO_3$ content, where *Microhedbergella praeplanispira* and *"Globigerinelloides" ultramicrus* are the most common species (Fig. 6, Supplementary Data Table 3).

The increase in diversity in the upper part of OAE 2 coincides with the occurrence of the trochospiral genera *Whiteinella* and *Praeglobotruncana*, the biserial *Planoheterohelix*, and (rarely) the double-keeled *Dicarinella*. *Whiteinella, Praeglobotruncana* and *Dicarinella* are more common in the large-sized fractions (>125 μm) whereas in the small-sized fractions (125–38 μm) *Muricohedbergella* progressively becomes the most abundant taxon present at the expense of *Microhedbergella.* In this interval *Planoheterohelix* together with *"Globigerinelloides"* occur as a minor component.

At the top of OAE 2 across the Cenomanian-Turonian boundary interval *Muricohedbergella delrioensis*, *Whiteinella baltica* and *Praeglobotruncana stephani* are the most common species and diversity ranges from 3 to 9 taxa. *Dicarinella hagni*, *Dicarinella canaliculata* and *Dicarinella imbricata* are all common elements present from the dicarinellid group (Supplementary Data Table 3).

A further increase in diversity of genera and species with the number of species ranging from 5 to 12 (Fig. 6) is registered in the Turonian and is characterized by the occurrence in the large-sized fractions of the double keeled genera *Marginotruncana* and *Falsotruncana* and of rare specimens of the single keeled *Helvetoglobotruncana*. Within the large-sized taxa *Marginotruncana coldreriensis* and *Marginotruncana pseudolinneiana* are the dominant species, and *Falsotruncana maslakovae* is the most common species among the falsotruncanid group. In this interval the small-sized species are composed mainly of *Microhedbergella praeplanispira* and *Muricohedbergella delrioensis*; *"Globigerinelloides" ultramicrus* and *Planoheterohelix* are a minor component. Even pooled together these small-sized taxa never reach the high absolute abundance values registered within the OAE 2 interval. The most important and common species are illustrated in Figs. 7 and 8.

8. Planktonic foraminiferal depth ecology

Information on planktonic foraminiferal paleoecology is provided by analyzing the interspecific patterns of offsets in $\delta^{18}O$ and $\delta^{13}C$ stable isotope ratios on well preserved specimens presented in this study (Fig. 9) and derived from the literature (e.g. D'Hondt and Arthur, 1995; Huber et al., 1995, 1999; Pearson et al., 2001; Wilson et al., 2002; Abramovich et al., 2003; Bornemann and Norris, 2007; Petrizzo et al., 2008; Ando et al., 2010; Wendler et al., 2013; MacLeod et al., 2013; Falzoni et al., 2013, 2014, 2016; Petrizzo et al., 2020).

Species-specific plots of $\delta^{18}O$ vs. $\delta^{13}C$ values can be used to interpret the foraminiferal depth ecology and infer variations in the vertical structure of the water column. Because sea surface temperatures are warmer than deeper waters and surface water dissolved inorganic carbon is depleted in ^{12}C by the activity of photosynthetic organisms (especially during the 'growing' season), taxa showing the lowest $\delta^{18}O$ and the highest $\delta^{13}C$ values are interpreted as surface dwellers. On the contrary, taxa displaying the highest $\delta^{18}O$ values and the lowest $\delta^{13}C$ values are interpreted deeper, thermocline dwellers, where the water is expected to be colder and where the oxidation of some of the sinking organic matter by bacteria has introduced ^{12}C-rich remineralized carbon to the DIC pool. Planktonic foraminiferal species adapted to shallow, warm, productive waters cluster in the upper right of the $\delta^{18}O$ vs. $\delta^{13}C$ foraminiferal cross plots and species adapted to colder, deeper depths plot in the bottom left (Pearson, 1998; Pearson et al., 2001). A well-defined separation among co-occurring taxa in isotope space is expected when the water masses are highly stratified and the thermocline is deep and well-developed, whereas lack of separation on one of both axes suggests less distinct niches. Planktonic foraminiferal taxa identified at Site U1516 are subdivided into mixed layer/surface, intermediate and thermocline dwellers according to the isotope signatures (Supplementary Data Table 3).

At Site U1516, the $\delta^{18}O$ vs. $\delta^{13}C$ foraminiferal cross-plot in the late Cenomanian highlights a small separation between surface and seafloor waters (471.41–487.64 m rCCSF, Fig. 9, Supplementary Data Table 2) either below the OAE 2 interval (473.94 to 487.64 m rCCSF, Fig. 2) or in the lower part of OAE 2 (471.41–473.47 m rCCSF, Fig. 2). The planktonic foraminifera *Whiteinella baltica* and *Muricohedbergella* sp. yield the lowest $\delta^{18}O$ and highest $\delta^{13}C$, and *W. baltica* shows a high intra-specific variability in $\delta^{18}O$ values among samples indicating a surface/summer and warmer mixed layer habitat. The high intra-specific variability in

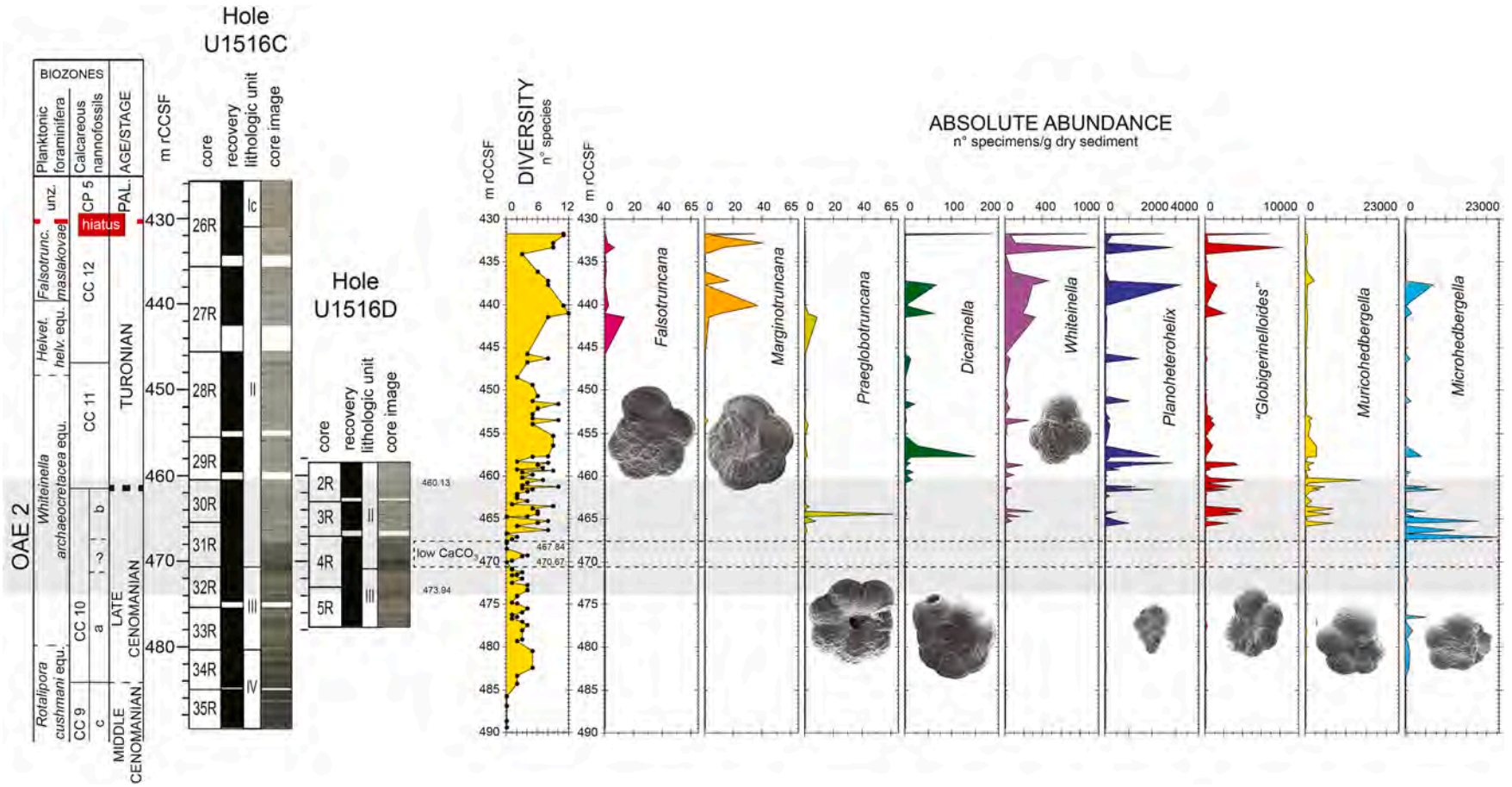

Fig. 6. Diversity and absolute abundance of planktonic foraminiferal genera in Holes U1516C and U1516D. Core recovery, lithologic units, core images and $CaCO_3$ according to Huber et al. (2019a). Planktonic foraminifera and calcareous nannofossil biostratigraphy from this study. The Cenomanian/Turonian boundary is approximated at the lowest occurrence of *Quadrum gartneri*. OAE 2 (gray band) is identified following Jarvis et al. (2011) Gambacorta et al. (2015) and Jenkyns et al. (2017). m rCCSF = revised Core Composite depth below Sea Floor in meters. See text for further explanation.

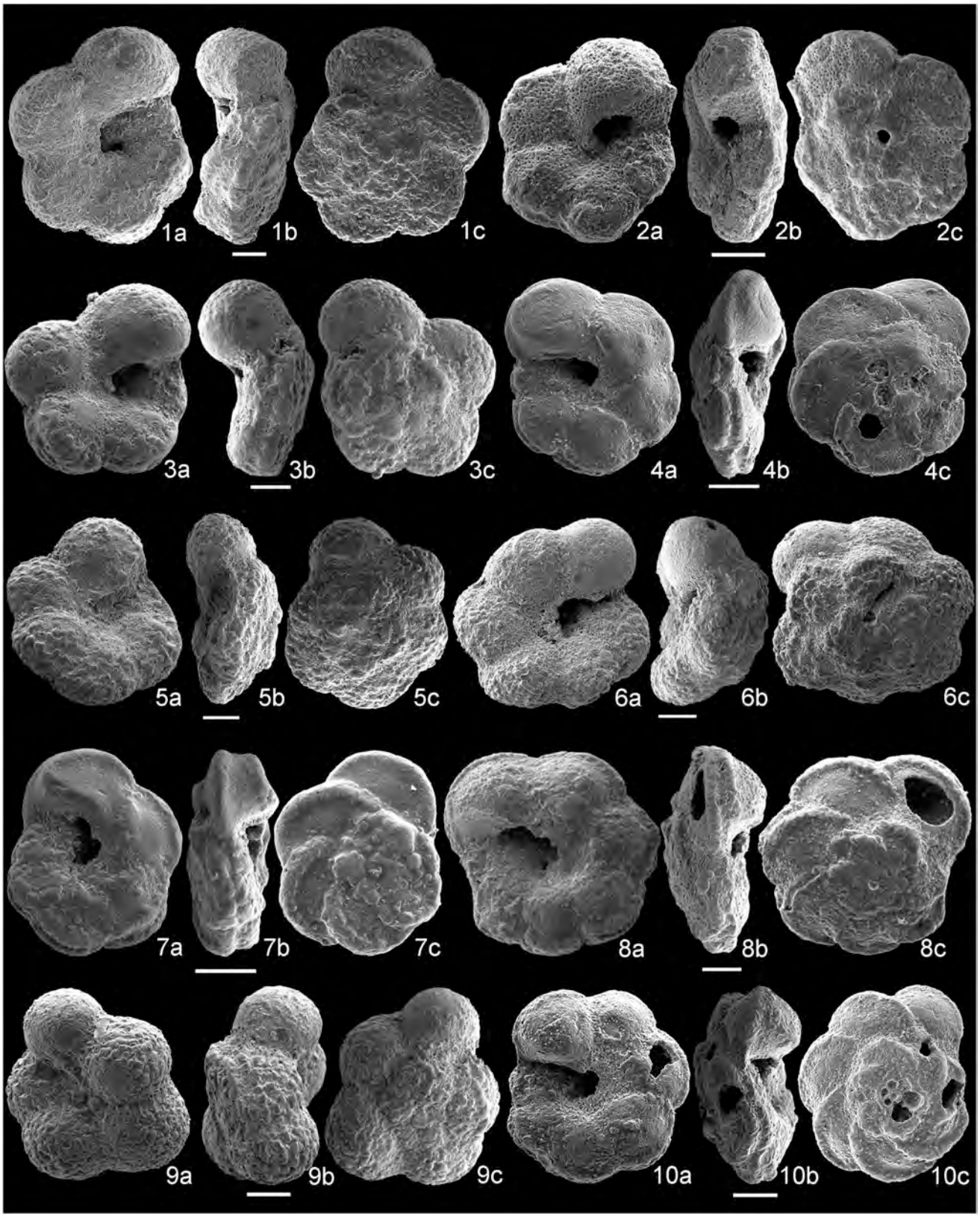

Fig. 7. Scanning Electron Microscope (SEM) images of species of planktonic foraminifera. 1a-c, *Falsotruncana maslakovae*, sample 369-U1516C-26R-4, 130–133 cm. 2a-c, *Falsotruncana douglasi*, sample 369-U1516C-27R-1, 7–10 cm. 3a-c, *Falsotruncana loeblichae*, sample 369-U1516C-27R-1, 7–10 cm. 4a-c, *Marginotruncana coldreriensis*, sample 369-U1516C-28R-3, 105–108 cm. 5a-c, *Praeglobotruncana stephani*, sample 369-U1516C-27R-4, 102–105 cm. 6a-c, *Praeglobotruncana gibba*, sample 369-U1516C-27R-4, 102–105 cm. 7a-c, *Marginotruncana pseudolinneiana*, sample 369-U1516C-28R-7, 10–13 cm. 8a-c, *Dicarinella hagni*, sample 369-U1516C-29R-3, 55–58 cm. 9a-c, *Helvetoglobotruncana praehelvetica*, sample 369-U1516C-29R-1, 5–8 cm. 10a-c, *Dicarinella hagni*, sample 369-U1516D-2R-3, 100–103 cm.
a, umbilical view; b, side view; c, spiral view. Scale bar 100 μm.

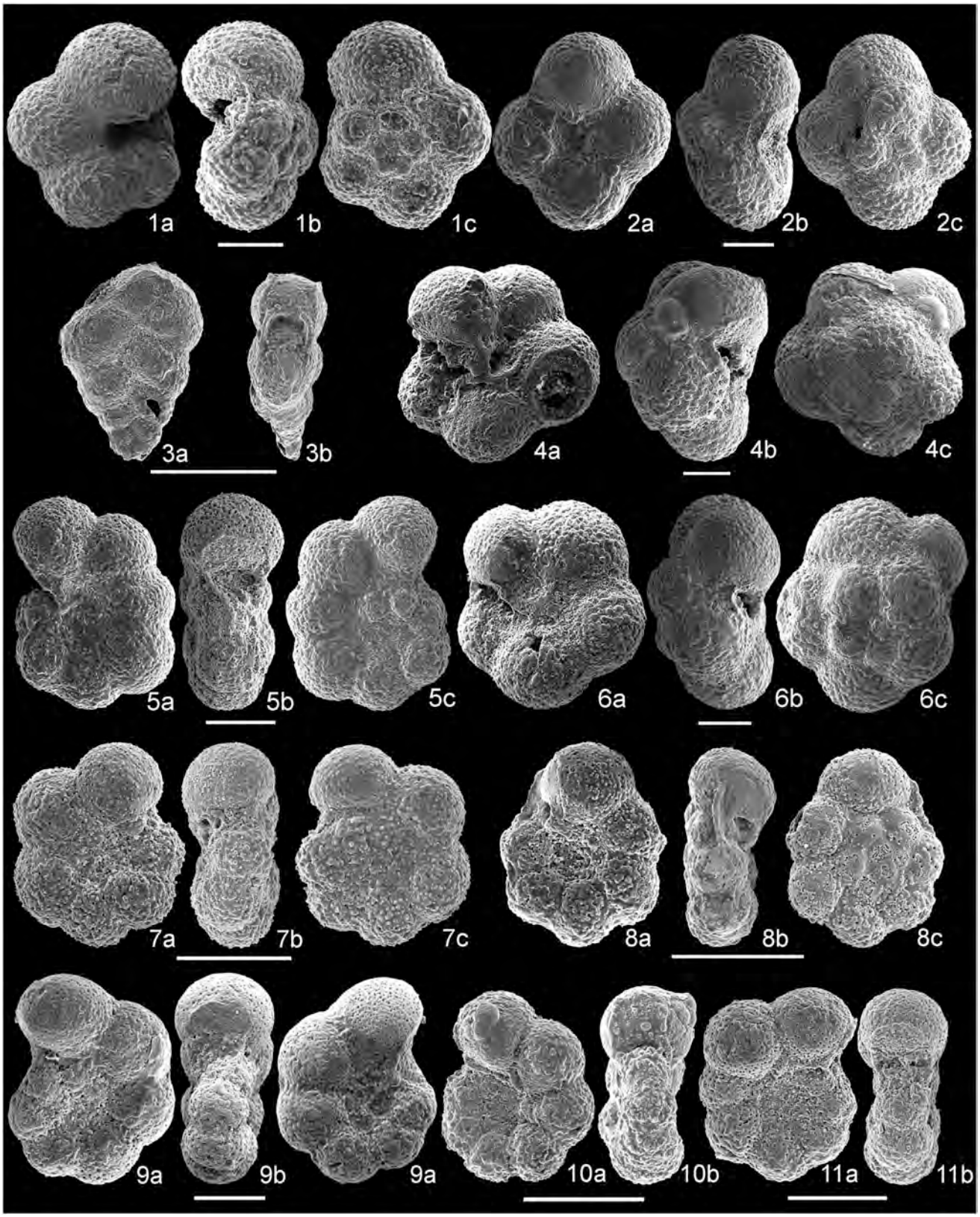

Fig. 8. Scanning electron microscope (SEM) images of species of planktonic foraminifera. 1a-c, *Muricohedbergella delrioensis*, sample 369-U1516C-30R-2, 2–5 cm. 2a-c, *Whiteinella baltica*, sample 369-U1516D-2R-3, 100–103 cm. 3a-c, *Planoheterohelix postmoremani*, sample 369-U1516C-26R-4, 112–115 cm. 4a-c, *Whiteinella paradubia*, sample 369-U1516D-2R-3, 100–103 cm. 5a-c, *Muricohedbergella planispira*, sample 369-U1516D-2R-4, 20–23 cm. 6a-c, *Whiteinella brittonensis*, sample 369-U1516D-2R-3, 100–103 cm. 7a-c, *Microhedbergella praeplanispira*, sample 369-U1516D-4R-5, 0–3 cm. 8a-c, *Microhedbergella praeplanispira*, sample 369-U1516C-33R-5, 3–7 cm. 9a-c, *"Globigerinelloides" bentonensis*, sample 32R-CC, 0–5 cm. 10a-b, *"Globigerinelloides" ultramicrus*, sample 369-U1516C-26R-4, 112–115 cm. 11a-b, "*Globigerinelloides" ultramicrus*, sample 369-U1516D-3R-1, 121–123 cm.
a, umbilical view; b, side view; c, spiral view. Scale bar 100 μm.

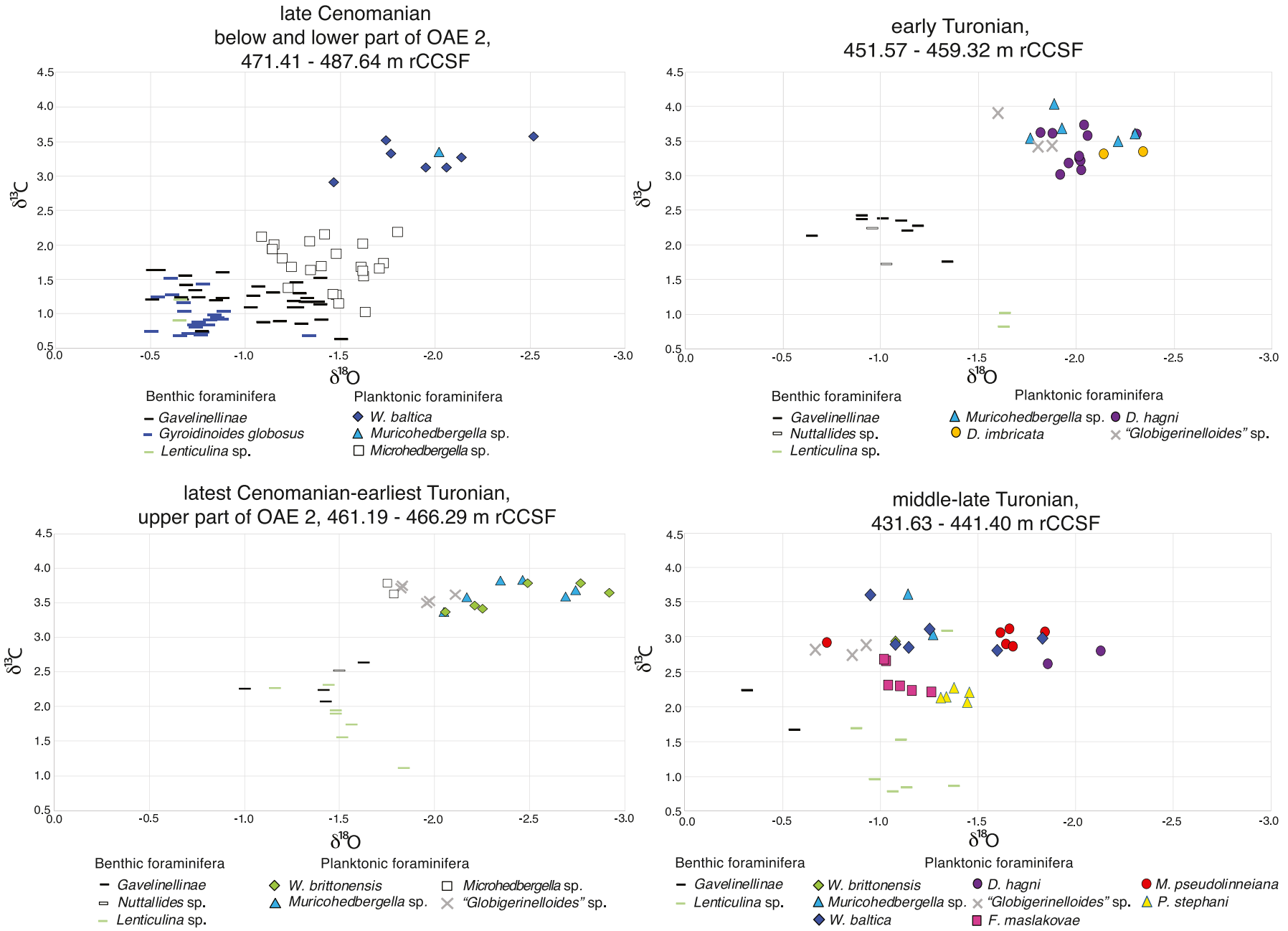

Fig. 9. $\delta^{18}O$ vs. $\delta^{13}C$ cross-plots of stable isotope values measured on well-preserved specimens from Holes U1516C and U1516D (Supplementary Data Table 2). See text for explanation of the intervals and interpretation of the depth ecologies of the taxa. m rCCSF = revised Core Composite depth below Sea Floor in meters.

$\delta^{18}O$ and $\delta^{13}C$ values of *Microhedbergella*, which is the most common planktonic foraminiferal genus occurring in this interval, suggests perturbations in temperature and nutrients concentrations indicating that this genus might either lived in the lower mixed layer or in the seasonal thermocline and is more adapted to winter/cooler habitat. Low $\delta^{13}C$ values seen in the small-sized *Microhedbergella* may reflect stronger disequilibrium fractionation due to their faster growth rate. Moreover, the small gradient in $\delta^{13}C$ values between benthic foraminifera and *Microhedbergella* could also reflect vertical mixing and upwelling.

The $\delta^{18}O$ vs. $\delta^{13}C$ foraminiferal cross-plot in the latest Cenomanian to earliest Turonian (461.19–466.29 m rCCSF, Fig. 9, Supplementary Data Table 2) highlights the lack of correlation between oxygen and carbon stable isotope data, which is due to the low $\delta^{13}C$ differentiation shown by the measured planktonic foraminiferal species. The geochemical distribution of $\delta^{13}C$ data during this interval is not consistent with a well-stratified water column. A possible explanation could be nutrient supply that would explain the presence of thermally stratified surface waters that lack a gradient in nutrient concentration. Seasonal variations in the surface waters are an additional source of variability in paleoecological interpretations (e.g., Petrizzo et al., 2008; Ando et al., 2010). *Whiteinella brittonensis* yields the lowest $\delta^{18}O$ and highest $\delta^{13}C$ values and shows the greater intra-specific variability in $\delta^{18}O$ values among samples consistent with a surface/summer mixed layer habitat. *Muricohedbergella* sp. shows an isotope signature suggesting they were adapted to the spring/winter mixed layer or lived near the seasonal thermocline. The two data points of *Microhedbergella* (at 463.76 and 465.22 m rCCSF, Figs. 2 and 9) show isotopic values indicating this genus might either lived in the winter mixed layer or in the seasonal thermocline. However, further high-resolution populations dynamics and geochemical analyses are needed to understand the paleoecology of the small-sized *Microhedbergella* and for interpreting the very low $\delta^{13}C$ values yielded in the underlying interval (below peak CIE and the interval of low $CaCO_3$ content, Figs. 2 and 9). Nevertheless, and despite the absence of a well-stratified water column and a defined thermocline, the $\delta^{18}O$ vs. $\delta^{13}C$ cross plot highlights a good separation between surface and seafloor waters.

In the early Turonian (451.57–459.32 m rCCSF, Fig. 9, Supplementary Data Table 2) the occurring planktonic foraminiferal taxa show $\delta^{18}O$ vs. $\delta^{13}C$ values similar to those observed in the previous interval with *Dicarinella imbricata* having an isotopic signature consistent with a preferred habitat in the spring/winter mixed layer or near the seasonal thermocline habitat. The less marked intraspecific variability in $\delta^{18}O$ values among samples shown by *Dicarinella hagni* and "*Globigerinelloides*" sp. may suggest they are intermediate dwellers that lived in the thick winter mixed layer or in the seasonal thermocline.

The degree of correlation between $\delta^{18}O$ and $\delta^{13}C$ values increase in the middle-late Turonian (431.63–441.40 m rCCSF, Fig. 9, Supplementary Data Table 2) and there is a moderate species separation in $\delta^{18}O$ and $\delta^{13}C$ space. These data are indicative of well-developed stratification, with a stable thermocline occupied by *Falsotruncana maslakovae* (Petrizzo et al., 2020) and *Praeglobotruncana stephani* (previously interpreted as intermediate dweller in Petrizzo et al., 2020) and a thick mixed layer inhabited by surface and intermediate species belonging to the genera "*Globigerinelloides*", *Dicarinella*, *Marginotruncana, Muricohedbergella* and *Whiteinella*. Specifically, the high intra-specific variability in $\delta^{18}O$ and $\delta^{13}C$ values of *Muricohedbergella* and *Whiteinella* suggests short term perturbations in temperature and nutrients concentrations indicating that these taxa might either lived in the mixed layer or above the seasonal thermocline. The co-occurring taxa show isotopic signatures consistent with depth habitats in the winter mixed layer or in the seasonal thermocline.

9. Paleotemperatures estimates

Planktonic and benthic paleotemperatures at Site U1516 are calculated from $\delta^{18}O$ values using the equations and adjustments explained in Huber et al. (2018) who analyzed the foraminiferal isotopic record from DSDP Sites 257 and 258 (southern Indian Ocean, Wharton and Mentelle Basin) and Site 511 (South Atlantic, Falkland Plateau) located at 60–62°S in the early Turonian.

At Site U1516 the $\delta^{18}O$ values of benthic and planktonic foraminifera in the interval below OAE 2 (from 473.94 to 487.64 m rCCSF) and in the lower part of the OAE 2 interval (from 471.41 to 473.47 m rCCSF) are generally higher than the data range of the $\delta^{18}O$ bulk carbonate (Fig. 2). In the interval coinciding with the lower OAE 2 (below peak CIE), benthic foraminiferal values range from −0.41 to −1.40‰ (13–16.5°C) and planktonic foraminifera range from −1.41 to −1.81‰ (16–19°C). The small-sized *Microhedbergella*, interpreted to be adapted to cooler waters, partially overlap with benthic foraminifera indicating a small separation between surface and seafloor waters temperatures.

In the upper part of OAE 2 (above the interval of low $CaCO_3$ content, from 463.76 to 466.29 m rCCSF) benthic foraminiferal values range from −1.16 to −1.57‰ (16–17.5°C) and planktonic foraminifera range from −1.75 to −2.74‰ (18–23°C), and they show a reduced vertical gradient in the column water at about 465 m rCCSF. Near the top of OAE 2 at the Cenomanian/Turonian boundary (at 461.19 m rCCSF), oxygen isotope ratios for planktonic foraminifera are notable for their remarkably low values of −2.05‰ to −2.91‰ that suggest paleotemperatures of 20–23.5°C (Fig. 2). The vertical gradient between sea surface and seafloor values is larger than the underlying interval as benthic foraminifera ranges from −1.0 to −1.48‰ (15–17°C).

In the early Turonian (456.40 to 459.32 m rCCSF) the vertical gradients between benthic and planktonic foraminifera increase to indicate a well stratified water column. Benthic foraminiferal values mostly range between −0.65‰ and − 1.19‰ (13–16°C) and planktonic foraminiferal values range between −1.60‰ and − 2.31‰ (17.6–21°C). In the overlying Turonian interval, the $\delta^{18}O$ values in core U1516C-28R (451.57–452.71 m rCCSF) indicate a good separation between sea surface and seafloor water masses as planktonic foraminiferal values range from −1.88‰ to −2.34‰ (19–21°C) and benthic foraminiferal range from −1.03‰ to −1.34‰ (15–16.5°C). Comparable values are observed in core U1516C-27R where planktonic foraminiferal values range from −1.08 to −2.13‰ (15°–20°C) and benthic foraminiferal values range from −0.32 to −1.35‰ (11°–16°C). The last sample analyzed in core U1516C-26R (431.63 m rCCSF) shows a convergence of planktonic and benthic foraminiferal values that could be related to increased diagenesis near the unconformity separating Cretaceous from Paleocene sediments or it might coincide with the onset of the cooling trend in the late Turonian (e.g., Clarke and Jenkyns, 1999; Huber et al., 2002; Cramer et al., 2009; Friedrich et al., 2012; Linnert et al., 2014).

Overall, the late Cenomanian-Turonian foraminiferal and bulk carbonate oxygen isotope ratios at Site U1516 reveal warmest paleotemperatures in the upper OAE 2 interval (late Cenomanian-early Turonian), followed by a progressive cooling during the Turonian. The good correspondence between $\delta^{18}O$ bulk carbonate and foraminiferal species-specific values obtained in the same samples at Site U1516 increases confidence in the reliability of both datasets (Fig. 2).

The bulk carbonate oxygen isotope record observed at Site U1516 only roughly correlates with the data from Eastbourne that show warming following the Plenus Cold Event and further warming after the termination of OAE 2 in the early Turonian (Fig. 2). In general, existing paleotemperature reconstructions from the Northern and Southern Hemispheres suggest that temperatures remained high throughout OAE 2 and into the early Turonian (Jenkyns et al., 1994; Huber et al., 1995; Norris and Wilson, 1998; Clarke and Jenkyns, 1999; Wilson et al., 2002; Schouten et al., 2003; Bice et al., 2003; Voigt et al., 2004; Forster et al., 2007; Bornemann et al., 2008; Pearce et al., 2009; Sinninghe Damsté et al., 2010; Jarvis et al., 2011; Friedrich et al., 2012; MacLeod et al., 2013; van Helmond et al., 2014; O'Brien et al., 2017; Huber et al., 2018; Robinson et al., 2019). This trend is less evident at Site U1516 (Holes U1516C-29R and U1516D-2R) where the early Turonian record suggests a slight decrease in surface and seafloor temperatures (assuming local

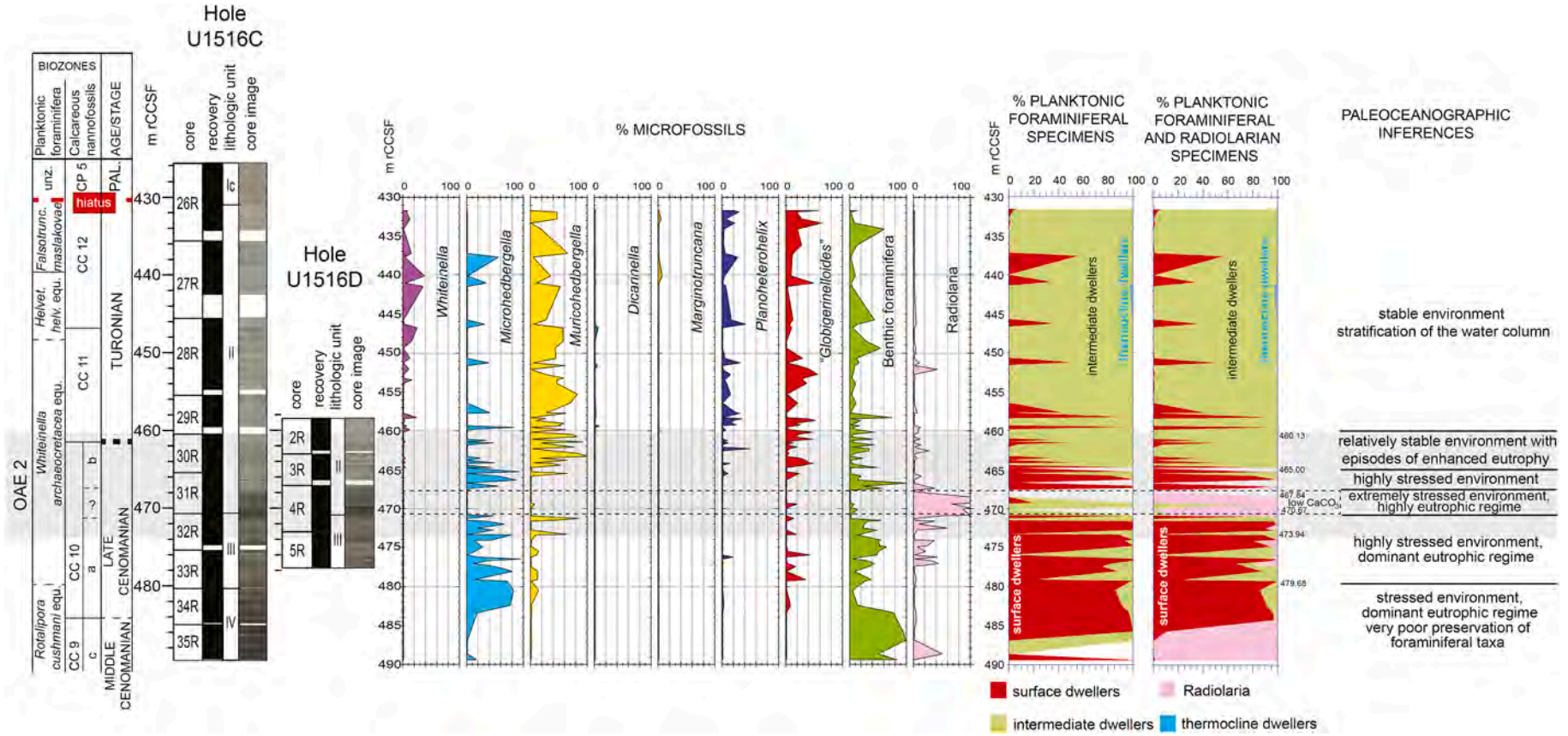

Fig. 10. Percent planktonic foraminifera, benthic foraminifera and radiolaria. Percent of surface, intermediate and thermocline dwellers planktonic foraminifera (Supplementary Data Table 3) used to derive the paleoceanographic interpretations in Holes 1516C and U15161D. Core recovery, lithologic units, core images and $CaCO_3$ according to Huber et al. (2019a). Planktonic foraminifera and calcareous nannofossil biostratigraphy from this study. The Cenomanian/Turonian boundary is approximated at the lowest occurrence of *Quadrum gartneri*. OAE 2 (gray band) is identified following Jarvis et al. (2011) Gambacorta et al. (2015) and Jenkyns et al. (2017). m rCCSF = revised Core Composite depth below Sea Floor in meters. See text for further explanation.

seawater $\delta^{18}O$ remain constant) compared to the warming values indicated at the termination of OAE 2 at Eastbourne (Fig. 2).

Data collected from DSDP Site 258 in the western Mentelle Basin, located only few km apart from Site U1516 (Fig. 1), record remarkably low planktonic and benthic $\delta^{18}O$ values (−3.76‰ and − 2.77‰, respectively) indicating warm sea surface and seafloor temperatures (27.5°C and 23°C, respectively) in the early Turonian calcareous nannofossils CC 11 Zone and just above a black shale bed that is correlated with OAE 2 (Huber et al., 2018), although marker species that biostratigraphically constrain the position of the Cenomanian/Turonian boundary and the OAE 2 are absent at the site. In the equivalent stratigraphic interval at Site U1516 (core 29R) planktonic foraminiferal values range between −1.60‰ and − 2.31‰ (17.6–21°C) and benthic foraminiferal values range between −0.65‰ and − 1.19‰ (13–16°C). The discrepancy of about 1.5‰ of the foraminiferal $\delta^{18}O$ values between the two sites is difficult to interpret and are additionally complicated by low recovery of sediments and low diversity of the calcareous plankton assemblages at Site 258 (Herb, 1974; Huber et al., 2018). The generally lower planktonic and benthic $\delta^{18}O$ values at Site 258 might also be related to the preservation of foraminifera characterized by diffuse overgrowths (Huber et al., 2018) compared to the specimens at Site U1516 that show only minor recrystallization in the equivalent time interval. A companion explanation could be the local oceanographic conditions at Site 258 differed from those at Site U1516. Site U1516 may have been characterized by episodes of upwelling as suggested by the occurrence of radiolaria (Fig. 5) (i.e., Casey, 1993; Premoli Silva et al., 1999; O'Dogherty and Guex, 2002) or of cooler bottom water; perhaps these cooler intervals were sampled in this study.

10. Paleoceanographic inferences

Changes in the composition and abundance of the microfossil assemblages combined with established paleoecological preferences of the planktonic foraminifera present are used to interpret the paleoceanographic features of the water column at Site U1516 with focus across OAE 2 and the overlying Turonian interval.

10.1. Stratigraphic interval below OAE 2 (473.94 to 489.42 m rCCSF)

The lithology in the stratigraphic interval in the middle and late Cenomanian (Figs. 2 and 10) from 479.68 to 489.42 m rCCSF in Hole U1516C cores 34R and 35R, is represented by mottled black clay-rich sediments (lithostratigraphic Unit IV; Huber et al., 2019a) with a relatively low carbonate content (Fig. 5; $CaCO_3$: 7.7 wt%). Microfossils in the mid-Cenomanian stratigraphic interval from core 35R include rare planktonic foraminifera and calcareous nannofossils, common benthic foraminifera and frequent radiolaria (Figs. 5, 6, and 10). The stratigraphic interval in core 34R, assigned to the early late Cenomanian, register an increase in planktonic foraminifera, whereas benthic foraminifera and radiolaria become rare (Figs. 5, 6, and 10). Nassellarian radiolaria are interpreted to be surface and subsurface dwellers that lived in shallow waters and their abundance in core 35R could reflect conditions of very high fertility (Lisitzin, 1985; Gowing, 1993; De Wever et al., 2003; Musavu-Moussavou et al., 2007). Increased productivity might have been caused by rise of the sea level in the middle-late Cenomanian (Haq, 2014) with expansion of the oxygen minimum zone and consequent loss of radiolaria with deeper habitats (Erbacher et al., 1996; Erbacher and Thurow, 1997). Warming and increased nutrient-rich runoff from the continent could be an alternative explanation.

Among planktonic foraminifera *Microhedbergella* is the most common genus in this interval, and it is often the only genus occurring near the top of core 35R and in core 34R. *Microhedbergella* is interpreted as an opportunistic small-sized taxon that likely may tolerate cooler and productive environments rich in nutrients; thus, its dominance in the assemblage could indicate the presence of an unstable and eutrophic water column especially in core 34R. However, interpreting the changes in microfossil composition in core 34R and 35R and the paleoceanographic setting is hampered by very low species richness. Nevertheless, the presence of planktonic foraminifera and radiolaria, that alternate and fluctuate in abundance, may indicate an open ocean setting in a relatively nearshore location, probably influenced by a combination of factors such as periodic upwelling, continental run off, sea level fluctuations, a shallow or expanded oxygen minimum zone, and markedly higher or lower salinity than normal marine conditions.

The interval from 473.94 to 479.68 m rCCSF (Fig. 10) yields a planktonic foraminiferal assemblage dominated by the opportunistic *Microhedbergella* whereas a minor component of the assemblages is represented by *Muricohedbergella* and *"Globigerinelloides"* that may have been intermediate dwellers (Norris and Wilson, 1998; Price et al., 1998; Wilson et al., 2002; Ando et al., 2010; Petrizzo et al., 2020; this study Figs. 6, 9, and 10). Benthic foraminifera fluctuate in abundance from 10% to 60% of the total microfossils and radiolaria vary from 5% at the base to 40% at the top of the interval. All together the variations in composition of the microfossil assemblages (Fig. 10) could correspond to times of enhanced surface water productivity or vertical mixing leading to a reduced water mass stratification as also indicated by overlap in the fields of isotopic values for planktonic and benthic foraminifera (Figs. 2 and 9). The horizons characterized by high abundance of benthic foraminifera (Fig. 10, 50–65% of the assemblages), from 474.02 to 477.32 m rCCSF, may coincide with episodes of re-oxygenation at the sea floor as the $\delta^{18}O$ bulk carbonate trend and the foraminiferal $\delta^{18}O$ values indicate cooler sea surface and bottom waters (Figs. 2 and 10).

10.2. Stratigraphic interval within OAE 2 (from 460.13 to 473.94 m rCCSF)

The dominance of the eutrophic regime continues until the lower part OAE 2 at 470.67 m rCCSF where surface dwelling radiolaria and *Microhedbergella* are common and benthic foraminifera range from 20% to 50% of the microfossil assemblages (Fig. 10). Although this stratigraphic interval coincides with a trough of the positive carbon excursion (P-CIE; O'Connor et al., 2020; Fig. 2) and with the highest $\delta^{18}O$ bulk carbonate and foraminiferal values observed within OAE 2, the microfossil assemblages show no evidence of abundances changes suggestive of a cooling event that would support the identification of the Plenus Cold Event (PCE, e.g., Jenkyns et al., 2017; Fig. 2) at Site U1516 (Fig. 10).

The middle part of the OAE 2 interval, from 467.84 to 470.67 m rCCSF, registers a change from biogenic carbonates to siliceous and organic matter-rich sediments characterized by low $CaCO_3$ content and by the near absence of calcareous planktonic and benthic foraminifera (Figs. 5 and 10). Except for a few samples that contain rare foraminifera, radiolaria are the sole microfossils present, and radiolaria have a peak in abundance at the highest TOC value at 469.95 m rCCSF (Figs. 5 and 10). Among planktonic foraminifera, species diversity is low (Fig. 6) and only rare representatives of the surface dweller *Whiteinella* and of the intermediate dwellers *Muricohedbergella* and *"Globigerinelloides"* (Huber et al., 1999; Petrizzo et al., 2020; this study) are recorded, whereas the small-sized *Microhedbergella* is almost absent. The abundance of radiolaria (albeit poorly preserved specimens) in this interval could reflect conditions of very high fertility and possibly shoaling of the Carbonate Compensation Depth (CCD). This interpretation agrees with the rarity and/or absence of calcareous foraminifera, and it suggests either dissolution of tests, especially of the small-sized and thin-walled *Microhedbergella*, induced by the strong oxidation of organic matter, or a very high surface water fertility that may have prevented survival of the foraminifera. Moreover, the maximum TOC values registered in this interval could indicate widespread organic matter deposition and expansion of anoxia at the sea floor coeval with an increase in productivity in the surface waters, as observed elsewhere in the Tethys region (e.g., Dolomites, Italy: Luciani and Cobianchi, 1999. Umbria-Marche Basin, Italy: Coccioni and Luciani, 2004, 2005. Tunisia: Nederbragt

and Fiorentino, 1999).

The microfossil record in this interval of Site U1516 is comparable with that of the Italian stratigraphic sections where foraminifera are absent in the organic-rich layers (Bonarelli Level) deposited during OAE 2 because of the absence of carbonate and the dominance of biogenica silica (e.g., Premoli Silva and Sliter, 1995; Premoli Silva et al., 1999; Scopelliti et al., 2004, 2008; Coccioni and Luciani, 2004, 2005; Mort et al., 2007; Coccioni and Premoli Silva, 2015). In the Umbria – Marche sections radiolaria show significant changes in abundance and assemblage composition (Marcucci Passerini et al., 1991; Erbacher and Thurow, 1997; O'Dogherty and Guex, 2002; Bąk, 2011) and the 60% of Cenomanian species went extinct during OAE 2, while the 50% of Turonian species first occurred during or just after the oceanic anoxic event. Investigating the radiolarian taxa composition and turnover at Site U1516 is beyond the scope of this study, however, similarly to the Italian sections (Musavu-Moussavou et al., 2007), we observed a dominance of Nassellarian radiolaria indicative of eutrophic conditions in the interval of low $CaCO_3$ content (Figs. 5 and 10). At Site U1516 the shift from carbonate-dominated plankton, which reduced the flux of calcium carbonate to the sea floor, and a rise in the CCD could have resulted from $CaCO_3$ undersaturation of waters due to prolonged ocean acidification during the thermal maximum and the $\delta^{13}C$ excursion (Fig. 2). These changes could have been forced by high atmospheric levels of CO_2 (Kuroda et al., 2007; Barclay et al., 2010; Gambacorta et al., 2015).

The return to carbonate deposition occurs in the upper part of OAE 2, from 460.13 to 467.84 m rCCSF, and is marked by high absolute abundance values of planktonic and benthic foraminifera (Figs. 5, 6 and 10). The lower part of this interval from 465 to 467.84 m rCCSF is characterized by a sudden increase in absolute abundance of small-sized *Microhedbergella*, paralleling an increase of benthic foraminifera and of $CaCO_3$ content, whereas small-sized radiolaria are present only as a minor component of the microfossil assemblages (Figs. 5, 6 and 10). *Microhedbergella* dominates the assemblages, which are characterized by strong cyclic fluctuations in absolute abundances of the planktonic and benthic foraminifera, with values ranging from zero to thousands of specimens (Figs. 5 and 6). The opportunistic *Microhedbergella* may have proliferated in high nutrient environments that, if coupled with low-oxygen conditions and higher atmospheric CO_2, may have led to even smaller-sized individuals as observed in this interval. Moreover, because of the rapid reproductive cycle and early sexual maturation, populations are composed of a very high number of specimens (Fig. 6). Thus, the dominance of *Microhedbergella* in the assemblage points to an unstable and highly eutrophic water column. Moreover, in this context *Microhedbergella* shows high $\delta^{18}O$ values (Figs. 2 and 9) that may indicate growth in cooler, eutrophic waters likely affected by upwelling of nutrient-rich and $\delta^{13}C$-depleted intermediate water masses with episodes of possible anoxia in the water column and at the sea floor because of the intensification of the oxygen minimum zone.

Higher in the interval characterized by the decreasing trend of $\delta^{13}C$ values (Fig. 2) and coinciding with the uppermost OAE 2 (from 460.13 to 465 m rCCSF), *Microhedbergella* abruptly decreases in absolute abundance and the assemblages become dominated by intermediate dwelling *Muricohedbergella* and *"Globigerinelloides"* (Figs. 6 and 10). Minor components in this interval are the surface dwelling *Whiteinella* and the biserial *Planoheterohelix* (Figs. 6 and 10). The latter taxon is interpreted to be an intermediate dweller adapted to a wide range of habitats from the mixed layer to the summer thermocline and/or relatively shoreward environments (Huber et al., 1995, 1999; MacLeod et al., 2001; Bornemann and Norris, 2007; Haynes et al., 2017; Petrizzo et al., 2020). *Planoheterohelix* is also reported occurring in high abundance in environmental settings characterized by very low oxygen conditions (i.e., *Heterohelix* shift at the Cenomanian/Turonian boundary. Western Interior Seaway, Leckie et al., 1998. Eastbourne, England, Keller et al., 2001. Umbria-Marche Basin, Italy, Coccioni and Luciani, 2004. Tunisia, Caron et al., 2006).

In the uppermost part of the OAE 2 interval, the composition of the planktonic foraminiferal assemblages together with the $\delta^{18}O$ vs. $\delta^{13}C$ foraminiferal cross-plot (Fig. 9) show a clear separation between benthic and planktonic foraminifera, which may indicate the presence of a defined temperature gradient between surface and bottom waters. The occurrence of rare keeled taxa (Fig. 6, *Dicarinella hagni*) usually regarded as intermediate or deep dwellers (Petrizzo et al., 2020; this study), could suggest periods of thermal separation between surface and thermocline waters with the development of a deep lower mixed layer. However, the low $\delta^{13}C$ differentiation shown by the planktonic foraminiferal species (Fig. 9) is not consistent with a well-stratified surface water column and may indicate eutrophic conditions that would have disrupted the nutricline. Moreover, species are thermally separated as shown by the $\delta^{18}O$ values ranging from −2.9‰ to −1.6‰ (Fig. 9) which is not expected in mixed conditions. A possible explanation invokes the episodic delivery of weathering or volcanically derived nutrients to the oceans as it would explain the presence of thermally stratified waters that lack a sharp gradient in the nutrient concentration.

10.3. Stratigraphic interval above OAE 2 (from 431.63 to 460.13 m rCCSF)

In the Turonian interval, above the OAE 2 interval and the $\delta^{13}C$ excursion, benthic and planktonic foraminifera fluctuate in abundance with the latter varying from 40% to 95% of the total microfossils (Figs. 5 and 10). Planktonic foraminifera increase in diversity with the progressive appearance of genera and species, indicating the presence of diverse ecological niches in the mixed layer and thermocline that were occupied by planktonic foraminifera possessing a wide range of trophic preferences (Figs. 6 and 10). The presence of a thick mixed layer is inferred by the isotopic signatures of *Whiteinella baltica*, *Dicarinella imbricata* and *Muricohedbergella* (Fig. 9), whereas *Dicarinella hagni* and *Marginotruncana pseudolinneiana* show a high degree of adaptation to different trophic regimes and are interpreted as intermediate dwellers living either within the mixed layer during cooler seasons or within the seasonal thermocline (Petrizzo et al., 2020; this study). Moreover, within the post-OAE 2 interval isotopic and faunal evidence suggest the presence of a well-stratified water column with relatively oligotrophic surface waters and a relatively stable thermocline suitable to the deep dwellers *Falsotruncana maslakovae* and *Praeglobotruncana stephani* (Figs. 6 and 9).

10.4. Remarks on the occurrences of Microhedbergella and Planoheterohelix

In general, as explained above, planktonic foraminiferal assemblages in the Mentelle Basin significantly differ from coeval assemblages at mid- to low latitudes either because of the absence of typical Tethyan species or because of differences in the stratigraphic distribution and absolute abundance values of some cosmopolitan taxa. For instance, at Site U1516 the small-sized and opportunistic *Microhedbergella* is the most abundant genus throughout OAE 2 and is replaced in absolute abundance by *Muricohedbergella* in the topmost part of the event. In the low latitude localities small-sized hedbergellids dominate within the Bonarelli Level in the Italian stratigraphic sections and have been interpreted as dwarfed specimens (Coccioni and Luciani, 2004, 2005) associated with high-surface productivity, low-oxygen conditions, and high atmospheric CO_2 to explain their small size.

Another example is the biserial *Planoheterohelix*, which at Site U1516 is a minor component of the assemblages within OAE 2 that became relatively common only in the overlying Turonian interval apparently without relation to any particular paleoceanographic change, although coinciding with the establishment of more stable conditions. On the contrary in low latitude records across the OAE 2, *Planoheterohelix* shows abrupt increases in abundance (*Heterohelix* shift: Leckie, 1985; Leckie et al., 1998) in some Tethyan (e.g., Eastbourne, England: Keller

et al., 2001. Tarfaya, Morocco: Falzoni et al., 2018. Umbria-Marche Basin, Italy: Coccioni and Luciani, 2004, 2005. Tunisia: Nederbragt and Fiorentino, 1999; Caron et al., 2006. Morocco: Keller et al., 2008) and Western Interior Seaway (Pueblo, Colorado: Leckie et al., 1998, Elderbak and Leckie, 2016) stratigraphic sections and, thus, is thought to be an opportunistic taxon that may proliferate in high productivity and low oxygen conditions. However, abrupt increase in biserials (i.e., *Planoheterohelix*, *Heterohelix*) has also been observed in normal environmental settings in the lower Turonian (Blake Nose, NW Atlantic Ocean: Huber et al., 1999) and upper Turonian (Tanzania: Haynes et al., 2015; Huber et al., 2017) confirming they were adapted to a wide range of habitats and water mass conditions. This discrepancy between the low and high latitude stratigraphic distributions and abundance of *Planoheterohelix* is difficult to interpret and could be ascribed to ecological factors (including apparently wide and flexible trophic preferences of species) and to different species adaptability to changes of the paleoceanographic parameters at different latitudes.

11. Conclusions

Site U1516 in the Mentelle Basin, located at 60–62°S in the mid-Cretaceous (Hay et al., 1999; Scotese, 2016; Müller et al., 2016) is to date the first austral locality where the Cenomanian/Turonian boundary and OAE 2 is documented with a detailed, integrated stratigraphic framework. It also represents the first high latitude locality in the Southern Hemisphere where planktonic foraminifera are consistently documented across the OAE 2 interval and the Cenomanian/Turonian boundary.

The carbon isotope record at Site U1516 is correlated with the $\delta^{13}C$ curve at Eastbourne, England (Tsikos et al., 2004) allowing identification of the increase, the plateau and the decrease phases of the $\delta^{13}C$ profile (Fig. 2). Integration of chemo- and biostratigraphic data through an age-depth model (Fig. 4) constrains the stage boundary and indicates that the record of OAE 2 is complete at Site U1516.

Detailed analysis of the microfossil assemblages provides insights on the paleoceanographic features of the perturbation associated with the global positive Carbon Isotope Excursion (CIE). The trough in the $\delta^{13}C$ profile and peak CIE that likely coincides with the P-CIE (O'Connor et al., 2020) and registers a $\delta^{18}O$ increase (Fig. 2), correlates at Site U1516 with an interval of eutrophic conditions in the surface waters (Fig. 10). Microfossil assemblages dominated by opportunistic radiolaria and small-sized *Microhedbergella* (Fig. 10), which may have flourished in high fertility environments and the species-specific $\delta^{18}O$ analyses (Fig. 2) may indicate cooling that could correspond to the Plenus Cold Event (e.g., Jenkyns et al., 2017), although no additional evidences of a cooling event are observed (Figs. 2 and 10).

The initiation of the plateau phase of the $\delta^{13}C$ profile that corresponds to the middle part of OAE 2 is masked at Site U1516 by the absence of carbonate coincident with the highest TOC values and the highest absolute abundance of radiolarians. Based on the microfossils assemblage, which is mainly composed by radiolaria, this interval is interpreted as an extremely stressed, highly eutrophic environment, with possible shoaling of the CCD (Fig. 10).

The upper part of OAE 2, characterized by the decrease phase in the $\delta^{13}C$ profile and $CaCO_3$ increase (Figs. 2 and 5), records an abrupt recovery and high absolute abundances values of the small-sized *Microhedbergella* and benthic foraminifera that show cyclic fluctuations similar to the lower part of OAE 2 (Fig. 10), and indicate an unstable environment in the surface water and at the sea floor likely affected by upwelling of nutrient-rich intermediate water masses with episodes of possible intensification of the oxygen minimum zone.

The topmost part of the OAE 2 interval contains more diverse planktonic foraminiferal assemblages still showing cyclic fluctuations in absolute abundances of specimens and characterized by a change in the composition of the assemblages with the intermediate dweller *Muricohedbergella*, which replaces the surface dweller and opportunistic *Microhedbergella* in absolute abundance. The foraminiferal data still reflect unstable surface water masses affected by cyclic nutrient enrichment, although the genera changeover and the occurrence of intermediate dwelling keeled taxa (*Dicarinella*) suggest phases of thermal separation within the upper column water with development of a thick mixed layer. Moreover, according to the $\delta^{18}O$ data from foraminiferal tests it also corresponds to the highest surface water paleotemperatures of 20°–23°C registered across the Cenomanian-Turonian boundary interval (Fig. 2).

In the Turonian interval after the termination of OAE 2, planktonic foraminiferal assemblages and the stable isotopes patterns indicate paleoceanographic conditions settled into a mesotrophic to oligotrophic regime characterized by a thermally stratified water column with a stable thermocline and a thick mixed layer.

The planktonic foraminiferal assemblages in the Mentelle Basin are significantly different from coeval assemblages at low latitudes because of the rarity and absence of many keeled thermocline dweller species. However, some similarities with the record from the Italian sections are observed, such as the occurrence of the small-sized *Microhedbergella*, which are equivalent to the dwarfed hedbergellids documented across the Bonarelli Level (Coccioni and Luciani, 2004, 2005) and regarded as indicative of high-surface productivity possibly coupled with depleted oxygen conditions. Among the remarkable discrepancies is the rarity of *Planoheterohelix* within OAE 2 in the Mentelle Basin while at low latitudes biserial taxa are common and often characterized by a shift to high abundance values in some localities (Leckie et al., 1998; Nederbragt and Fiorentino, 1999; Keller et al., 2001; Caron et al., 2006; Keller et al., 2008; Falzoni et al., 2016), which have been correlated to low oxygen conditions.

Finally, the microfossils and stable isotopic data presented in this paper nicely document the paleoceanographic changes across the OAE 2 interval and the Cenomanian/Turonian boundary. Although interpretations in some stratigraphic intervals may be limited by combined complications of the scarcity of microfossil taxa, low diversity of planktonic foraminifera, and low carbonate content likely due to shoaling of the CCD and consequent ocean acidification, Site U1516 provides the first complete OAE 2 record at southern high latitudes. The data presented provide a broad and detailed perspective on the paleoceanographic evolution of the region. Further studies of the same stratigraphic interval at the nearby Site U1513, located at a deeper water depth (2800 m, Huber et al., 2019c) compared to U1516 (2600 m, Huber et al., 2019a), will complement the results presented here.

Declaration of Competing Interest

The authors declare that they have no known competing financial interests or personal relationships that could have appeared to influence the work reported in this paper.

Acknowledgements

We warmly thank the editor Fabienne Marret-Davies and two anonymous reviewers for their helpful comments and suggestions. This research used data and samples provided by the International Ocean Discovery Program (IODP). MRP acknowledge financial support by IODP-Italia and CNR-Italian National Research Council (projects CONTR_CNR19MPETR_01 and CONTR_CNR17MPETR_01) to perform activities related to ECORD (European Consortium for Ocean Research Drilling) e IODP, and by the Italian Ministry of University and Research (MIUR), projects PRIN 2017RX9XXY (E. Erba scientific coordinator) and Dipartimenti di Eccellenza 2018–2022, Le Geoscienze per la Società: Risorse e loro evoluzione. BTH, KGM, and DKW acknowledge that funding for this project was provided by United States Science Support Program of the International Ocean Discovery Program. TH acknowledges research funds provided by Japan Drilling Earth Sciences Consortium (JDESC) and by Japan Society for the Promotion of Sciences

(JSPS) KARENHI Grant number 19H02011.

Appendix A. Supplementary data

Supplementary data to this article can be found online at https://doi.org/10.1016/j.gloplacha.2021.103595.

References

Abramovich, S., Keller, G., Stüben, D., Berner, Z., 2003. Characterization of late Campanian and Maastrichtian planktonic foraminiferal depth habitats and vital activities based on stable isotopes. Palaeogeogr. Palaeoclimatol. Palaeoecol. 202, 1–29.

Adams, D.D., Hurtgen, M.T., Sageman, B.B., 2010. Volcanic triggering of a biogeochemical cascade during Oceanic Anoxic Event 2. Nat. Geosci. 3, 201–204.

Ando, A., Huber, B.T., MacLeod, K.G., 2010. Depth-habitat reorganization of planktonic foraminifera across the Albian/Cenomanian boundary. Paleobiology 36, 357–373.

Arthur, M.A., Schlanger, S.T., Jenkyns, H.C., 1987. The Cenomanian-Turonian Oceanic Anoxic Event, II. Palaeoceanographic controls on organic-matter production and preservation. Geol. Soc. Lond. Spec. Publ. 26, 401–420.

Bąk, M., 2011. Tethyan radiolarians at the Cenomanian-Turonian Anoxic Event from the Apennines (Umbria-Marche) and the Outer Carpathians: palaeoecological and palaeoenvironmental implications. Stud. Geol. Pol. 134, 5–279.

Barclay, R.S., McElwain, J.C., Sageman, B.B., 2010. Carbon sequestration activated by a volcanic CO_2 pulse during Ocean Anoxic Event 2. Nat. Geosci. 3, 205–208.

Batenburg, S.J., De Vleeschouwer, D., Sprovieri, M., Hilgen, F.J., Gale, A.S., Singer, B.S., Koeberl, C., Coccioni, R., Claeys, P., Montanari, A., 2016. Orbital control on the timing of oceanic anoxia in the Late Cretaceous. Clim. Past 12 (10), 1995–2009.

Bice, K.L., Huber, B.T., Norris, R.D., 2003. Extreme polar warmth during the Cretaceous greenhouse? Paradox of the late Turonian $\delta^{18}O$ record at Deep Sea Drilling Project Site 511. Paleoceanography 18 (2), 1031.

Bjerrum, C.J., Bendtsen, J., Legarth, J.J.F., 2006. Modeling organic carbon burial during sea level rise with reference to the Cretaceous. Geochem. Geophys. Geosyst. 7 (5), Q05008.

Blättler, C.L., Jenkyns, H.C., Reynard, L.M., Henderson, G.M., 2011. Significant increases in global weathering during Oceanic Anoxic Events 1a and 2 indicated by calcium isotopes. Earth Planet. Sci. Lett. 309 (1–2), 77–88.

Bomou, B., Adatte, T., Tantawy, A.A., Mort, H., Fleitmann, D., Huang, Y., Föllmi, K.B., 2013. The expression of the Cenomanian–Turonian oceanic anoxic event in Tibet. Palaeogeogr. Palaeoclimatol. Palaeoecol. 369, 466–481.

Bornemann, A., Norris, R.D., 2007. Size-related stable isotope changes in Late Cretaceous planktic foraminifera: implications for paleoecology and photosymbiosis. Mar. Micropaleontol. 65, 32–42.

Bornemann, A., Norris, R.D., Friedrich, O., Beckmann, B., Schouten, S., Damsté, J.S.S., Vogel, J., Hofmann, P., Wagner, T., 2008. Isotopic evidence for glaciation during the Cretaceous supergreenhouse. Science 319 (5860), 189–192.

Bowman, A.R., Bralower, T.J., 2005. Paleoceanographic significance of high-resolution carbon isotope records across the Cenomanian–Turonian boundary in the Western Interior and New Jersey coastal plain, USA. Mar. Geol. 217 (3–4), 305–321.

Caron, M., Dall'Agnolo, S., Accarie, H., Barrera, E., Kauffman, E.G., Amédro, F., Robaszynski, F., 2006. High-resolution stratigraphy of the Cenomanian–Turonian boundary interval at Pueblo (USA) and wadi Bahloul (Tunisia): stable isotope and bio-events correlation. Geobios 39, 171–200.

Casey, R.E., 1993. Radiolaria. In: Lipps, J.H. (Ed.), Fossil Prokaryotes and Protists. Blackwell Science Publisher, pp. 249–284.

Charbonnier, G., Adatte, T., Spangenberg, J.E., Föllmi, K.B., 2018. The expression of early Aptian to latest Cenomanian oceanic anoxic events in the sedimentary record of the Briançonnais domain. Glob. Planet. Chang. 170, 76–92.

Clarke, L.J., Jenkyns, H.C., 1999. New oxygen isotope evidence for long-term Cretaceous climatic change in the Southern Hemisphere. Geology 27, 699–702.

Coccioni, R., Luciani, V., 2004. Planktonic foraminifera and environmental changes across the Bonarelli Event (OAE2, latest Cenomanian) in its type area: a high resolution study from the Tethyan reference Bottaccione section (Gubbio, central Italy). J. Foraminifer. Res. 34, 109–129.

Coccioni, R., Luciani, V., 2005. Planktonic foraminifers across the Bonarelli Event (OAE2, latest Cenomanian): the Italian record. Palaeogeogr. Palaeoclimatol. Palaeoecol. 224, 167–185.

Coccioni, R., Premoli Silva, I., 2015. Revised Upper Albian–Maastrichtian planktonic foraminiferal biostratigraphy and magnetostratigraphy of the classical Tethyan Gubbio section (Italy). Newsl. Stratigr. 48, 47–90. https://doi.org/10.1127/nos/2015/0055.

Corbett, M.J., Watkins, D.K., Pospichal, J.J., 2014. A quantitative analysis of calcareous nannofossil bioevents of the Late Cretaceous (Late Cenomanian–Coniacian) Western Interior Seaway and their reliability in established zonation schemes. Mar. Micropaleontol. 109, 30–45.

Cramer, B.S., Toggweiler, J.R., Wright, J.D., Katz, M.E., 2009. Ocean overturning since the Late Cretaceous: inferences from a new benthic foraminiferal isotope compilation. Paleoceanography 24, PA4216. https://doi.org/10.1029/2008PA001683.

De Wever, P., O'Dogherty, L., Caridroit, M., Dumitrica, P., Guex, J., Nigrini, C., Caulet, J. P., 2003. Diversity of radiolarian families through time. Bull. Soc. Géol. Fr. 174 (5), 453–469.

Desmares, D., Grosheny, D., Beaudoin, B., Gardin, S., Gauthier-Lafaye, F., 2007. High resolution stratigraphic record constrained by volcanic ashes layers at the Cenomanian-Turonian boundary in the Western Interior Basin, USA. Cretac. Res. 28, 561–582.

Desmares, D., Crognier, N., Bardin, J., Testé, M., Beaudoin, B., Grosheny, D., 2016. A new proxy for Cretaceous paleoceanographic and paleoclimatic reconstructions: coiling direction changes in the planktonic foraminifera *Muricohedbergella delrioensis*. Palaeogeogr. Palaeoclimatol. Palaeoecol. 445, 8–17.

D'Hondt, S., Arthur, M.A., 1995. Interspecies variation in stable isotopic signals of Maastrichtian planktonic foraminifera. Paleoceanography 10 (1), 123–135.

Dickson, A.J., Saker-Clarket, M., Jenkyns, H.C., Bottini, C., Erba, E., Russo, F., Gorbanenko, O., Naafs, B.D.A., Pancost, R.D., Robinson, S.A., van Den Boorn, S.H.J. M., Idiz, E., 2017. A Southern Hemisphere record of global trace-metal drawdown and orbital modulation of organic-matter burial across the Cenomanian-Turonian boundary (Ocean Drilling Program Site 1138, Kerguelen Plateau). Sedimentology 64, 186–203.

Dixon, M., Haig, D.W., Mory, A.J., Backhouse, J., Ghori, K.A.R., Howe, R., Morris, P.A., 2003. GSWA Edaggee 1 well completion report (interpretive), Gascoyne Platform, Southern Carnarvon Basin, Western Australia. Geol. Surv. W. Aust. Rec. 8, 1–80.

Du Vivier, A.D.C., Selby, D., Sageman, B.B., Jarvis, I., Gröcke, D.R., Voigt, S., 2014. Marine $^{187}Os/^{188}Os$ isotope stratigraphy reveals the interaction of volcanism and ocean circulation during Oceanic Anoxic Event 2. Earth Planet. Sci. Lett. 389, 23–33.

Eicher, D.L., Diner, R., 1985. Foraminifera as indicators of water mass in the Cretaceous Greenhorn Sea, Western Interior. In: Pratt, L.M., Kauffman, E.G., Zelt, F.B. (Eds.), Fine-Grained Deposits and Biofacies of the Cretaceous Western Interior Seaway: Evidence of Cyclic Sedimentary Processes, Field Trip Guidebook, 4. Society of Economic Paleontologists and Mineralogists, pp. 60–71.

Eicher, D.L., Worstell, P., 1970. Cenomanian and Turonian foraminifera from the Great Plains, United States. Micropaleontology 16, 269–324.

Elderbak, K., Leckie, R.M., 2016. Paleocirculation and foraminiferal assemblages of the Cenomanian–Turonian Bridge Creek Limestone bedding couplets: productivity vs. dilution during OAE2. Cretac. Res. 60, 52–77.

Eldrett, J.S., Minisini, D., Bergman, S.C., 2014. Decoupling of the carbon cycle during Ocean Anoxic Event 2. Geology 42 (7), 567–570.

Eldrett, J.S., Dodsworth, P., Bergman, S.C., Wright, M., Minisini, D., 2017. Water-mass evolution in the Cretaceous Western Interior Seaway of North America and equatorial Atlantic. Clim. Past 13 (7), 855–878.

Erba, E., 2004. Calcareous nannofossils and Mesozoic oceanic anoxic events. Mar. Micropaleontol. 52, 85–106.

Erbacher, J., 2021. Data report: radiolarians from the latest Cenomanian and Turonian, Holes U1512A and U1516C, IODP Expedition 369. In: Hobbs, R.W., Huber, B.T., Bogus, K.A., the Expedition 369 Scientists, Australia Cretaceous Climate and Tectonics (Eds.), Proceedings of the International Ocean Discovery Program, 369: College Station, TX (International Ocean Discovery Program). https://doi.org/10.14379/iodp.proc.369.203.2021.

Erbacher, J., Thurow, J., 1997. Influence of oceanic anoxic events on the evolution of mid-Cretaceous radiolaria in the North Atlantic and western Tethys. Mar. Micropaleontol. 30 (1–3), 139–158.

Erbacher, J., Thurow, J., Littke, R., 1996. Evolution patterns of radiolaria and organic matter variations: a new approach to identify sea-level changes in mid-Cretaceous pelagic environments. Geology 24, 499–502.

Erbacher, J., Friedrich, O., Wilson, P.A., Birch, H., Mutterlose, J., 2005. Stable organic carbon isotope stratigraphy across Oceanic Anoxic Event 2 of Demerara Rise, western tropical Atlantic. Geochem. Geophys. Geosyst. 6 (6), Q06010.

Falzoni, F., Petrizzo, M.R., 2020. Patterns of planktonic foraminiferal extinctions and eclipses during Oceanic Anoxic Event 2 at Eastbourne (SE England) and other mid-low latitude locations. Cretac. Res. 104593 https://doi.org/10.1016/j.cretres.2020.104593.

Falzoni, F., Petrizzo, M.R., MacLeod, K.G., Huber, B.T., 2013. Santonian-Campanian planktonic foraminifera from Tanzania, Shatsky Rise and Exmouth Plateau: species depth ecology and paleoceanographic inferences. Mar. Micropaleontol. 103, 15–29. https://doi.org/10.1016/j.marmicro.2013.07.003.

Falzoni, F., Petrizzo, M.R., Huber, B.T., MacLeod, K.G., 2014. Insights into the meridional ornamentation of the planktonic foraminiferal genus *Rugoglobigerina* (Late Cretaceous) and implications for taxonomy. Cretac. Res. 47, 87–104. https://doi.org/10.1016/j.cretres.2013.11.001.

Falzoni, F., Petrizzo, M.R., Clarke, L.C., MacLeod, K.G., Jenkyns, H.J., 2016. Long-term Late Cretaceous carbon- and oxygen-isotope trends and planktonic foraminiferal turnover: a new record from the southern mid-latitudes. GSA Bull. 128, 1725–1735. https://doi.org/10.1130/B31399.1.

Falzoni, F., Petrizzo, M.R., Caron, M., Leckie, R.M., Elderbak, K., 2018. Age and synchronicity of planktonic foraminiferal bioevents across the Cenomanian–Turonian boundary interval (Late Cretaceous). Newsl. Stratigr. 51, 343–380. https://doi.org/10.1127/nos/2018/0416.

Forster, A., Schouten, S., Baas, M., Sinninghe Damsté, J.S., 2007. Mid-Cretaceous (Albian–Santonian) sea surface temperature record of the tropical Atlantic Ocean. Geology 35, 919–922.

Forster, A., Kuypers, M.M.M., Turgeon, S.C., Brumsack, H.-J., Petrizzo, M.R., Sinninghe Damsté, J.S., 2008. The Cenomanian/Turonian oceanic anoxic event in the South Atlantic: new insights by a geochemical study of DSDP Leg 75 Site 530A. Palaeogeogr. Palaeoclimatol. Palaeoecol. 267, 256–283.

Friedrich, O., Erbacher, J., Mutterlose, J., 2006. Paleoenvironmental changes across the Cenomanian/Turonian boundary event (oceanic anoxic event 2) as indicated by benthic foraminifera from the Demerara Rise (ODP Leg 207). Rev. Micropaleontol. 49 (3), 121–139.

Friedrich, O., Norris, R.D., Erbacher, J., 2012. Evolution of middle to Late Cretaceous oceans – a 55 my record of Earth's temperature and carbon cycle. Geology 40 (2), 107–110.
Frijia, G., Parente, M., 2008. Strontium isotope stratigraphy in the upper Cenomanian shallow-water carbonates of the southern Apennines: short-term perturbations of marine $^{87}Sr/^{86}Sr$ during the oceanic anoxic event 2. Palaeogeogr. Palaeoclimatol. Palaeoecol. 261 (1–2), 15–29.
Gaer, B.T., Watkins, D.K., 2020. A biometric analysis of the *Eiffellithus eximius* species complex and its biostratigraphic implications. Mar. Micropaleontol. 157, 101876.
Gale, A.S., Christensen, W.K., 1996. Occurrence of the belemnite *Actinocamax plenus* in the Cenomanian of SE France and its significance. Bull. Geol. Soc. Den. 43, 68–77.
Gale, A.S., Kennedy, W.J., Voigt, S., Walaszczyk, I., 2005. Stratigraphy of the Upper Cenomanian-Lower Turonian Chalk succession at Eastbourne, Sussex, UK: ammonites, inoceramid bivalves and stable carbon isotopes. Cretac. Res. 26, 460–487.
Gale, A.S., Jenkyns, H.C., Tsikos, H., van Breugel, Y., Sinninghe Damsté, J.S., Bottini, C., Erba, E., Russo, F., Falzoni, F., Petrizzo, M.R., Dickson, A.J., Wray, D.S., 2019. High-resolution bio- and chemostratigraphy of an expanded record of Oceanic Anoxic Event 2 (Late Cenomanian-Early Turonian) at Clot Chevalier, near Barrême, SE France (Vocontian Basin, SE France). Newsl. Stratigr. 52, 97–129. https://doi.org/10.1127/nos/2018/0445.
Gambacorta, G., Jenkyns, H.C., Russo, F., Tsikos, H., Wilson, P.A., Faucher, G., Erba, E., 2015. Carbon-and oxygen-isotope records of mid-Cretaceous Tethyan pelagic sequences from the Umbria-Marche and Belluno Basins (Italy). Newsl. Stratigr. 48 (3), 299–323.
Gangl, S.K., Moy, C.M., Stirling, C.H., Jenkyns, H.C., Crampton, J.S., Clarkson, M.O., Ohneiser, C., Porcelli, D., 2019. High-resolution records of Oceanic Anoxic Event 2: insights into the timing, duration and extent of environmental perturbations from the palaeo-South Pacific Ocean. Earth Planet. Sci. Lett. 518, 172–182.
Gavrilov, Y.O., Shcherbinina, E.A., Golovanova, O.V., Pokrovskii, B.G., 2013. The late Cenomanian paleoecological event (OAE 2) in the eastern Caucasus basin of Northern Peri-Tethys. Lithol. Miner. Resour. 48 (6), 457–488.
Gebhardt, H., Friedrich, O., Schenk, B., Fox, L., Hart, M., Wagreich, M., 2010. Paleoceanographic changes at the northern Tethyan margin during the Cenomanian–Turonian Oceanic Anoxic Event (OAE-2). Mar. Micropaleontol. 77 (1–2), 25–45.
Govindan, A., Ramesh, P., 1995. Cretaceous anoxic events and their role in generation and accumulation of hydrocarbons in Cauvery Basin, India. Indian J. Pet. Geol. 4, 1–15.
Gowing, M.M., 1993. Seasonal radiolarian flux at the VERTEX North Pacific time-series site. Deep. Res. I Oceanogr. Res. Pap. 40, 517–545.
Gradstein, F.M., Ogg, J.G., Schmitz, M.D., Ogg, G.M., 2012. The Geologic Time Scale 2012. Elsevier, Oxford, UK, p. 1144.
Grosheny, D., Beaudoin, B., Morel, L., Desmares, D., 2006. High-resolution biostratigraphy and chemostratigraphy of the Cenomanian–Turonian Boundary Event in the Vocontian Basin, S-E France. Cretac. Res. 27, 629–640.
Grosheny, D., Ferry, S., Lecuyer, C., Thomas, A., Desmares, D., 2017. The Cenomanian–Turonian Boundary Event (CTBE) on the southern slope of the Subalpine Basin (SE France) and its bearing on a probable tectonic pulse on a larger scale. Cretac. Res. 72, 39–65.
Haig, D.W., Mory, A.J., Backhouse, J., Campbell, R.J., Ghori, K.A.R., Howe, R., Morris, P. A., 2004. GSWA Boologooro 1 well completion report (interpretive), southern Carnarvon Basin, Western Australia. Geol. Surv. W. Aust. Rec. 4, 1–106.
Haq, B.U., 2014. Cretaceous eustasy revisited. Glob. Planet. Chang. 113, 44–58.
Hardas, P., Mutterlose, J., Friedrich, O., Erbacher, J., 2012. The Middle Cenomanian Event in the equatorial Atlantic: the calcareous nannofossil and benthic foraminiferal response. Mar. Micropaleontol. 96, 66–74.
Hart, M.B., Leary, P.N., 1989. The stratigraphic and palaeogeographic setting of the late Cenomanian 'anoxic' event. J. Geol. Soc. Lond. 146, 305–310.
Hart, M.B., Leary, P.N., 1991. Stepwise mass extinctions: the case for the Late Cenomanian event. Terra Nova 3 (2), 142–147.
Hart, M.B., Weaver, P.P.E., 1977. Turonian microbiostratigraphy of Beer, SE Devon. Proc. Ussher Soc. 4, 86–93.
Hart, M.B., Monteiro, J.F., Watkinson, M.P., Price, G.D., 2002. Correlation of events at the Cenomanian/Turonian boundary: evidence from Southern England and Colorado. In: Wagreich, M. (Ed.), Aspects of Cretaceous Stratigraphy and Palaeobiogeography.Schriftenreihe der erdwissenschaftliche Kommission der Österreichische Akademie der Wissenschaften, 15. Verlag der Österreichische Akademie der Wissenschaften, Wien, pp. 35–46.
Hasegawa, T., 1999. Planktonic foraminifera and biochronology of the Cenomanian-Turonian (Cretaceous) sequence in the Oyubari area, Hokkaido, Japan. Paleontol. Res. 3, 173–192.
Hasegawa, T., Seo, S., Moriya, K., Tominaga, Y., Nemoto, T., Naruse, T., 2010. High resolution carbon isotope stratigraphy across the Cenomanian/Turonian boundary in the Tappu area, Hokkaido, Japan: correlation with world reference sections. Sci. Rep. Kanazawa Univ. 54, 49–62.
Hasegawa, T., Crampton, J.S., Schiøler, P., Field, B., Fukushi, K., Kakizaki, Y., 2013. Carbon isotope stratigraphy and depositional oxia through Cenomanian/Turonian boundary sequences (Upper Cretaceous) in New Zealand. Cretac. Res. 40, 61–80.
Hay, W.W., DeConto, R., Wold, C.N., Wilson, K.M., Voigt, S., Schulz, M., Wold-Rossby, A., Dullo, W.C., Ronov, A.B., Balukhovsky, A.N., Soeding, E., 1999. Alternative global Cretaceous paleogeography. In: Barrera, E., Johnson, C.C. (Eds.), The evolution of the Cretaceous Ocean/Climate System, 332. Geological Society of America Special Paper, Boulder, Colorado, pp. 1–47.
Haynes, S.J., Huber, B.T., MacLeod, K.G., 2015. Evolution and phylogeny of mid-Cretaceous (Albian-Coniacian) biserial planktic foraminifera. J. Foraminifer. Res. 45, 42–81.
Haynes, S.J., MacLeod, K.G., Huber, B.T., Warny, S., Kaufman, A.J., Pancost, R.D., Jiménez Berrocoso, Á., Petrizzo, M.R., Watkins, D.K., Zhelezinskaia, I., 2017. Depositional environments, marine and terrestrial links, and exceptional preservation in the Turonian of southeastern Tanzania. Geol. Soc. Am. Bull. 129, 515–533. https://doi.org/10.1130/B31432.1.
Heimhofer, U., Wucherpfennig, N., Adatte, T., Schouten, S., Schneebeli-Hermann, E., Gardin, S., Keller, G., Kentsch, S., Kujau, A., 2018. Vegetation response to exceptional global warmth during Oceanic Anoxic Event 2. Nat. Commun. 9 (1), 1–8.
Herb, R., 1974. Cretaceous Planktonic Foraminifera from the Eastern Indian Ocean. Initial Report of the Deep Sea Drilling Project 26. U.S. Government Printing Office, Washington, D.C., pp. 745–770
Higgins, M.B., Robinson, R.S., Husson, J.M., Carter, S.J., Pearson, A., 2012. Dominant eukaryotic export production during Ocean Anoxic Events reflects the importance of recycled NH_4^+. Proc. Natl. Acad. Sci. 109 (7), 2269–2274.
Huber, B.T., Petrizzo, M.R., 2014. Evolution and taxonomic study of the Cretaceous planktic foraminiferal genus *Helvetoglobotruncana* Reiss, 1957. J. Foraminifer. Res. 44, 40–57.
Huber, B.T., Hodell, D.A., Hamilton, C.P., 1995. Middle-Late Cretaceous climate of the southern high latitudes: stable isotopic evidence for minimal equator-to-pole thermal gradients. Geol. Soc. Am. Bull. 107, 1164–1191.
Huber, B.T., Leckie, R.M., Norris, R.D., Bralower, T.J., CoBabe, E., 1999. Foraminiferal assemblage and stable isotopic change across the Cenomanian–Turonian boundary in the subtropical North Atlantic. J. Foraminifer. Res. 29, 392–417.
Huber, B.T., Norris, R.D., MacLeod, K.G., 2002. Deep-sea paleotemperature record of extreme warmth during the Cretaceous. Geology 30, 123–126.
Huber, B.T., Petrizzo, M.R., Young, J.R., Falzoni, F., Gilardoni, S.E., Bown, P.R., Wade, B. S., 2016. Pforams@ microtax. Micropaleontology 62 (6), 429–438.
Huber, B.T., Petrizzo, M.R., Watkins, D.K., Haynes, S.J., MacLeod, K.G., 2017. Correlation of Turonian continental margin and deep-sea sequences in the subtropical Indian Ocean sediments by integrated planktonic foraminiferal and calcareous nannofossil biostratigraphy. Newsl. Stratigr. 50 (2), 141–185. https://doi.org/10.1127/nos/2017/0373.
Huber, B.T., MacLeod, K.G., Watkins, D.K., Coffin, M.F., 2018. The rise and fall of the Cretaceous hot greenhouse climate. Glob. Planet. Chang. 167, 1–23.
Huber, B.T., Hobbs, R.W., Bogus, K.A., Batenburg, S.J., Brumsack, H.-J., do Monte Guerra, R., Edgar, K.M., Edvardsen, T., Garcia Tejada, M.L., Harry, D.L., Hasegawa, T., Haynes, S.J., Jiang, T., Jones, M.M., Kuroda, J., Lee, E.Y., Li, Y.-X., MacLeod, K.G., Maritati, A., Martinez, M., O'Connor, L.K., Petrizzo, M.R., Quan, T. M., Richter, C., Riquier, L., Tagliaro, G.T., Wainman, C.C., Watkins, D.K., White, L.T., Wolfgring, E., Xu, Z., 2019a. Site U1516. In: Hobbs, R.W., Huber, B.T., Bogus, K.A., the Expedition 369 Scientists, Australia Cretaceous Climate and Tectonics (Eds.), Proceedings of the International Ocean Discovery Program, 369: College Station, TX (International Ocean Discovery Program). https://doi.org/10.14379/iodp.proc.369.107.2019.
Huber, B.T., Hobbs, R.W., Bogus, K.A., Batenburg, S.J., Brumsack, H.-J., do Monte Guerra, R., Edgar, K.M., Edvardsen, T., Garcia Tejada, M.L., Harry, D.L., Hasegawa, T., Haynes, S.J., Jiang, T., Jones, M.M., Kuroda, J., Lee, E.Y., Li, Y.-X., MacLeod, K.G., Maritati, A., Martinez, M., O'Connor, L.K., Petrizzo, M.R., Quan, T. M., Richter, C., Riquier, L., Tagliaro, G.T., Wainman, C.C., Watkins, D.K., White, L.T., Wolfgring, E., Xu, Z., 2019b. Expedition 369 methods. In: Hobbs, R.W., Huber, B.T., Bogus, K.A., the Expedition 369 Scientists, Australia Cretaceous Climate and Tectonics (Eds.), Proceedings of the International Ocean Discovery Program, 369: College Station, TX (International Ocean Discovery Program). https://doi.org/10.14379/iodp.proc.369.102.2019.
Huber, B.T., Hobbs, R.W., Bogus, K.A., Batenburg, S.J., Brumsack, H.-J., do Monte Guerra, R., Edgar, K.M., Edvardsen, T., Garcia Tejada, M.L., Harry, D.L., Hasegawa, T., Haynes, S.J., Jiang, T., Jones, M.M., Kuroda, J., Lee, E.Y., Li, Y.-X., MacLeod, K.G., Maritati, A., Martinez, M., O'Connor, L.K., Petrizzo, M.R., Quan, T. M., Richter, C., Riquier, L., Tagliaro, G.T., Wainman, C.C., Watkins, D.K., White, L.T., Wolfgring, E., Xu, Z., 2019c. Site U1513. In: Hobbs, R.W., Huber, B.T., Bogus, K.A., the Expedition 369 Scientists, Australia Cretaceous Climate and Tectonics (Eds.), Proceedings of the International Ocean Discovery Program, 369: College Station, TX (International Ocean Discovery Program). https://doi.org/10.14379/iodp.proc.369.104.2019.
Jarvis, I., Gale, A.S., Jenkyns, H.C., Pearce, M.A., 2006. Secular variation in Late Cretaceous carbon isotopes: a new $\delta^{13}C$ carbonate reference curve for the Cenomanian–Campanian (99.6–70.6 Ma). Geological Magazine 143 (5), 561–608.
Jarvis, I., Lignum, J.S., Gröcke, D.R., Jenkyns, H.C., Pearce, M.A., 2011. Black shale deposition, atmospheric CO2 drawdown, and cooling during the Cenomanian–Turonian Oceanic Anoxic Event. Paleoceanography 26, PA3201. https://doi.org/10.1029/2010PA002081.
Jefferies, R.P.S., 1963. The stratigraphy of the *Actinocamax plenus* subzone (Turonian) in the Anglo-Paris Basin. Proc. Geol. Assoc. 74 (1), 1-IN4.
Jenkyns, H.C., 2003. Evidence for rapid climate change in the Mesozoic–Palaeogene greenhouse world. Philos. Trans. R. Soc. Lond. A Math. Phys. Eng. Sci. 361 (1810), 1885–1916.
Jenkyns, H.C., 2010. Geochemistry of oceanic anoxic events. Geochem. Geophys. Geosyst. 11, Q03004. https://doi.org/10.1029/2009GC002788.
Jenkyns, H.C., Gale, A.S., Corfield, R.M., 1994. Carbon-and oxygen-isotope stratigraphy of the English Chalk and Italian Scaglia and its palaeoclimatic significance. Geol. Mag. 131 (1), 1–34.
Jenkyns, H.C., Dickson, A.J., Ruhl, M., Boorn, S.H., 2017. Basalt-seawater interaction, the Plenus Cold Event, enhanced weathering and geochemical change:

deconstructing Oceanic Anoxic Event 2 (Cenomanian–Turonian, Late Cretaceous). Sedimentology 64, 16–43.
Joo, Y.J., Sageman, B.B., 2014. Cenomanian to Campanian carbon isotope chemostratigraphy from the Western Interior Basin, USA. J. Sediment. Res. 84 (7), 529–542.
Joo, Y.J., Sageman, B.B., Hurtgen, M.T., 2020. Data-model comparison reveals key environmental changes leading to Cenomanian-Turonian Oceanic Anoxic Event 2. Earth Sci. Rev. 203, 103123.
Kalanat, B., Gharaie, M.H.M., Vahidinia, M., Matsumoto, R., 2018. Short-term eustatic sea-level changes during the Cenomanian–Turonian Supergreenhouse interval in the Kopet-Dagh Basin, NE Tethyan realm. J. Iber. Geol. 44 (2), 177–191.
Keller, G., Pardo, A., 2004. Age and paleoenvironment of the Cenomanian-Turonian global stratotype section and point at Pueblo, Colorado. Mar. Micropaleontol. 51, 95–128.
Keller, G., Han, Q., Adatte, T., Burns, S., 2001. Paleoenvironment of the Cenomanian-Turonian transition at Eastbourne, England. Cretac. Res. 22, 391–422.
Keller, G., Adatte, T., Berner, Z., Chellai, E.H., Stueben, D., 2008. Oceanic events and biotic effects of the Cenomanian-Turonian anoxic event, Tarfaya Basin, Morocco. Cretac. Res. 29, 976–994.
Keller, G., Nagori, M.L., Chaudhary, M., Reddy, A.N., Jaiprakash, B.C., Spangenberg, J. E., Mateo, P., Adatte, T., 2021. Cenomanian-Turonian sea-level transgression and OAE 2 deposition in the Western Narmada Basin, India. Gondwana Res. 94, 73–86.
Kennedy, W.J., Walaszczyk, I., Cobban, W.A., 2000. Pueblo, Colorado, USA, candidate Global Boundary Stratotype Section and Point for the base of the Turonian Stage of the Cretaceous, and for the base of the Middle Turonian Substage, with a revision of the Inoceramidae (Bivalvia). Acta Geol. Pol. 5 (3), 295–334.
Kennedy, W.J., Walaszczyk, I., Cobban, W.P., 2005. The Global Boundary Stratotype Section and Point for the base of the Turonian Stage of the Cretaceous: Pueblo, Colorado, USA. Episodes 28, 93–104.
Kerr, A.C., 1998. Oceanic plateau formation: a cause of mass extinction and black shale deposition around the Cenomanian–Turonian boundary? J. Geol. Soc. 155 (4), 619–626.
Kolonic, S., Wagner, T., Forster, A., Sinninghe Damsté, J.S., Walsworth-Bell, B., Erba, E., Turgeon, S., Brumsack, H.-J., Chellai, E.H., Tsikos, H., Kuhnt, W., Kuypers, M.M.M., 2005. Black shale deposition on the northwest African Shelf during the Cenomanian/Turonian oceanic anoxic event: climate coupling and global organic carbon burial. Paleoceanography 20 (1), PA1006. https://doi.org/10.1029/2003PA000950.
Kuhnt, W., Luderer, F., Nederbragt, S., Thurow, J., Wagner, T., 2005. Orbital-scale record of the late Cenomanian–Turonian oceanic anoxic event (OAE-2) in the Tarfaya Basin (Morocco). Int. J. Earth Sci. 94 (1), 147–159.
Kuhnt, W., Holbourn, A.E., Beil, S., Aquit, M., Krawczyk, T., Flögel, S., Chellai, E.H., Jabour, H., 2017. Unraveling the onset of Cretaceous Oceanic Anoxic Event 2 in an extended sediment archive from the Tarfaya-Laayoune Basin, Morocco. Paleoceanography 32 (8), 923–946.
Kuroda, J., Ogawa, N.O., Tanimizu, M., Coffin, M.F., Tokuyama, H., Kitazato, H., Ohkouchi, N., 2007. Contemporaneous massive subaerial volcanism and Late Cretaceous Oceanic Anoxic Event 2. Earth Planet. Sci. Lett. 256 (1–2), 211–223.
Kuypers, M.M.M., Pancost, R.D., Damste, J.S.S., 1999. A large and abrupt fall in atmospheric CO_2 concentration during Cretaceous times. Nature 399 (6734), 342–345.
Kuypers, M.M.M., Pancost, R.D., Nijenhuis, I.A., Sinninghe Damsté, J.S., 2002. Enhanced productivity led to increased organic carbon burial in the euxinic North Atlantic basin during the late Cenomanian oceanic anoxic event. Paleoceanography 17 (4), 1051.
Lamolda, M.A., Gorostidi, A., Martínez, R., López, G., Peryt, D., 1997. Fossil occurrences in the Upper Cenomanian-Lower Turonian at Ganuza, northern Spain: an approach to Cenomanian/Turonian boundary chronostratigraphy. Cretac. Res. 18 (3), 331–353.
Larson, R.L., 1991. Latest pulse of the Earth: evidence for a mid-Cretaceous super plume. Geology 19, 547–550.
Larson, R.L., Erba, E., 1999. Onset of the Mid-Cretaceous greenhouse in the Barremian-Aptian: igneous events and the biological, sedimentary, and geochemical responses. Paleoceanography 14 (6), 663–678.
Leckie, R.M., 1985. Foraminifera of the Cenomanian–Turonian boundary interval, Greenhorn Formation, Rock Canyon Anticline, Pueblo, Colorado. In: Pratt, L.M., Kauffman, E.G., Zelt, F.B. (Eds.), Fine-Grained Deposits and Biofacies of the Cretaceous Western Interior Seaway: Evidence of Cyclic Sedimentary Processes, Field Trip Guidebook, 4. Society of Economic Paleontologists and Mineralogists, pp. 139–149.
Leckie, R.M., Bralower, T.J., Cashman, R., 2002. Oceanic anoxic events and plankton evolution: biotic response to tectonic forcing during the mid-Cretaceous. Paleoceanography 17. https://doi.org/10.1029/2001PA000623.
Leckie, R.M., Yuretrich, R.F., West, O.L.O., Finkelstein, D., Schmidt, M., 1998. Paleoceanography of the southwestern Western Interior Sea during the time of the Cenomanian–Turonian boundary (Late Cretaceous). In: Dean, W., Arthur, M.A. (Eds.), Stratigraphy and Paleoenvironments of the Cretaceous Western Interior Seaway, SEPM Concepts in Sedimentology and Paleontology, 6, pp. 101–126.
Linnert, C., Mutterlose, J., Erbacher, J., 2010. Calcareous nannofossils of the Cenomanian/Turonian boundary interval from the Boreal Realm (Wunstorf, northwest Germany). Mar. Micropaleontol. 74, 38–58.
Linnert, C., Mutterlose, J., Mortimore, R., 2011. Calcareous nannofossils from Eastbourne (southeastern England) and the paleoceanography of the Cenomanian–Turonian Boundary interval. Palaios 26, 298–313.
Linnert, C., Robinson, S., Lees, J., Bown, P., Pérez-Rodríguez, I., Petrizzo, M.R., Falzoni, F., Littler, K., Arz, J., Russell, E., 2014. Evidence for global cooling in the Late Cretaceous. Nat. Commun. 5, 4194. https://doi.org/10.1038/ncomms5194.
Lisitzin, A.P., 1985. The silica cycle during the last ice age. Palaeogeogr. Palaeoclimatol. Palaeoecol. 50 (1), 241–270.
Lowery, C.M., Leckie, R.M., 2017. Biostratigraphy of the Cenomanian-Turonian Eagle Ford Shale of south Texas. J. Foraminifer. Res. 47, 105–128.
Luciani, V., Cobianchi, M., 1999. The Bonarelli level and other black shales in the Cenomanian-Turonian of the northeastern Dolomites (Italy): calcareous nannofossil and foraminiferal data. Cretac. Res. 20, 135–167.
MacLeod, K.G., Huber, B.T., Pletsch, T., Röhl, U., Kucera, M., 2001. Maastrichtian foraminiferal and paleoceanographic changes on Milankovitch time scales. Paleoceanography 16, 133–154.
MacLeod, K.G., Martin, E.E., Blair, S.W., 2008. Nd isotopic excursion across Cretaceous Ocean Anoxic Event 2 (Cenomanian-Turonian) in the tropical North Atlantic. Geology 36, 811–814. https://doi.org/10.1130/G24999A.1.
MacLeod, K.G., Huber, B.T., Jiménez Berrocoso, Á., Wendler, I., 2013. A stable and hot Turonian without glacial $\delta^{18}O$ excursions is indicated by exquisitely preserved Tanzanian foraminifera. Geology 41 (10), 1083–1086. https://doi.org/10.1130/G34510.1.
Marcucci Passerini, M., Bettini, P., Dainelli, J., Sirugo, A., 1991. The "Bonarelli Horizon" in the central Apennines (Italy): radiolarian biostratigraphy. Cretac. Res. 12 (3), 321–331.
Martin, E.E., MacLeod, K.G., Jiménez Berrocoso, Á., Bourbon, E., 2012. Water mass circulation on Demerara rise during the Late Cretaceous based on Nd isotopes. Earth Planet. Sci. Lett. 327–328, 111–120. https://doi.org/10.1016/j.epsl.2012.01.037.
Mitchell, R.N., Bice, D.M., Montanari, A., Cleaveland, L.C., Christianson, K.T., Coccioni, R., Hinnov, L.A., 2008. Oceanic anoxic cycles? Orbital prelude to the Bonarelli level (OAE 2). Earth Planet. Sci. Lett. 267 (1–2), 1–16.
Monteiro, F.M., Pancost, R.D., Ridgwell, A., Donnadieu, Y., 2012. Nutrients as the dominant control on the spread of anoxia and euxinia across the Cenomanian-Turonian Oceanic Anoxic Event (OAE2): model-data comparison. Paleoceanography 27 (4), PA4209. https://doi.org/10.1029/2012PA002351.
Moriya, K., Wilson, P.A., Friedrich, O., Erbacher, J., Kawahata, H., 2007. Testing for ice sheets during the mid-Cretaceous greenhouse using glassy foraminiferal calcite from the mid-Cenomanian tropics on Demerara Rise. Geology 35 (7), 615–618.
Mort, H., Jacquat, O., Adatte, T., Steinmann, P., Föllmi, K., Matera, V., Berner, Z., Stüben, D., 2007. The Cenomanian/Turonian anoxic event at the Bonarelli Level in Italy and Spain: enhanced productivity and/or better preservation? Cretac. Res. 28, 597–612.
Müller, R.D., Seton, M., Zahirovic, S., Williams, S.E., Matthews, K.J., Wright, N.M., Shephard, G.E., Maloney, K.T., Barnett-Moore, N., Hosseinpour, M., Bower, D.J., Cannon, J., 2016. Ocean basin evolution and global-scale plate reorganization events since Pangea breakup. Annu. Rev. Earth Planet. Sci. 44 (1), 107–138.
Musavu-Moussavou, B., Danelian, T., Baudin, F., Coccioni, R., Fröhlich, F., 2007. The Radiolarian biotic response during OAE2. A high-resolution study across the Bonarelli level at Bottaccione (Gubbio, Italy). Rev. Micropaleontol. 50 (3), 253–287.
Nederbragt, A.J., Fiorentino, A., 1999. Stratigraphy and palaeoceanography of the Cenomanian–Turonian Boundary Event in Oued Mellegue, north-western Tunisia. Cretac. Res. 20, 47–62.
Norris, R.D., Wilson, P.A., 1998. Low-latitude sea- surface temperatures for the mid-Cretaceous and the evolution of planktic foraminifera. Geology 26, 823–826.
O'Brien, C.L., Robinson, S.A., Pancost, R.D., Sinningeh Damsté, J.S., Schoulten, S., Lunt, D.J., Alsenz, H., Bornemann, A., Bottini, C., Brassell, S.C., Farnsworth, A., Forster, A., Huber, B.T., Inglis, G.N., Jenkyns, H.C., Linnert, C., Littler, K., Markwick, P., McAnena, A., Mutterlose, J., Naafs, B.D.A., Püttmann, W., Sluis, A., van Helmond, N.A.G.M., Vellekoop, J., Wagner, T., Wrobel, N.E., 2017. Cretaceous sea-surface temperature evolution: constraints from TEX_{86} and planktonic foraminiferal oxygen isotopes. Earth Sci. Rev. 172, 224–247.
O'Connor, L.K., Jenkyns, H.C., Robinson, S.A., Remmelzwaal, S.R., Batenburg, S.J., Parkinson, I.J., Gale, A.S., 2020. A re-evaluation of the Plenus Cold Event, and the links between CO_2, temperature, and seawater chemistry during OAE 2. Paleoceanogr. Paleoclimatol. 35 https://doi.org/10.1029/2019PA003631 e2019PA003631.
O'Dogherty, L., Guex, J., 2002. Rates and pattern of evolution among Cretaceous radiolarians: relations with global paleoceanographic events. Micropaleontology 48, 1–22.
Olayiwola, M.A., Bamford, M.K., Durugbo, E.U., 2017. Graphic correlation: A powerful tool for biostratigraphic correlation of petroleum exploration and production in the Cenozoic deep offshore Niger Delta, Nigeria. Journal of African Earth Sciences 131, 156–165.
Owens, J.D., Gill, B.C., Jenkyns, H.C., Bates, S.M., Severmann, S., Kuypers, M.M.M., Woodfine, R.G., Lyons, T.W., 2013. Sulfur isotopes track the global extent and dynamics of euxinia during Cretaceous Oceanic Anoxic Event 2. Proc. Natl. Acad. Sci. 110 (46), 18407–18412.
Pancost, R.D., Crawford, N., Magness, S., Turner, A., Jenkyns, H.C., Maxwell, J.R., 2004. Further evidence for the development of photic-zone euxinic conditions during Mesozoic oceanic anoxic events. J. Geol. Soc. 161, 353–364.
Parente, M., Frijia, G., Di Lucia, M., Jenkyns, H.C., Woodfine, R.G., Baroncini, F., 2008. Stepwise extinction of larger foraminifers at the Cenomanian-Turonian boundary: a shallow-water perspective on nutrient fluctuations during Oceanic Anoxic Event 2 (Bonarelli Event). Geology 36 (9), 715–718.
Paul, C.R.C., Lamolda, M.A., 2009. Testing the precision of bioevents. Geological Magazine 625–637.
Paul, C.R.C., Lamolda, M.A., Mitchell, S.F., Vaziri, M.R., Gorostidi, A., Marshall, J.D., 1999. The Cenomanian–Turonian boundary at Eastbourne (Sussex, UK): a proposed European reference section. Palaeogeogr. Palaeoclimatol. Palaeoecol. 150, 83–121.
Pearce, M.A., Jarvis, I., Tocher, B.A., 2009. The Cenomanian–Turonian boundary event, OAE2 and palaeoenvironmental change in epicontinental seas: new insights from the

dinocyst and geochemical records. Palaeogeogr. Palaeoclimatol. Palaeoecol. 280, 207–234.
Pearson, P.N., 1998. Stable isotopes and the study of evolution in planktonic foraminifera. Paleontol. Soc. Pap. 4, 138–178.
Pearson, P.N., Ditchfield, P.W., Singano, J.M., Harcourt-Brown, K.G., Nicholas, C.J., Olsson, R.K., Shackleton, N.J., Hall, M.A., 2001. Warm tropical sea surface temperatures in the Late Cretaceous and Eocene Epochs. Nature 413, 481–487. https://doi.org/10.1038/35097000.
Perch-Nielsen, K., 1985. Mesozoic calcareous nannofossils. Plankton Stratigr. 329–426.
Petrizzo, M.R., 2001. Late Cretaceous planktonic foraminifera from Kerguelen Plateau (ODP Leg 183): new data to improve the Southern Ocean biozonation. Cretac. Res. 22, 829–855. https://doi.org/10.1006/cres.2001.0290.
Petrizzo, M.R., 2003. Late Cretaceous planktonic foraminiferal bioevents in the Tethys and in the Southern Ocean record: an overview. J. Foraminifer. Res. 33 (4), 330–337. https://doi.org/10.2113/0330330.
Petrizzo, M.R., Huber, B.T., Wilson, P.A., MacLeod, K.G., 2008. Late Albian paleoceanography of the western subtropical North Atlantic. Paleoceanography 23, PA1213. https://doi.org/10.1029/2007PA001517.
Petrizzo, M.R., Jiménez Berrocoso, Á., Falzoni, F., Huber, B.T., MacLeod, K.G., 2017. The Coniacian–Santonian sedimentary record in southern Tanzania (Ruvuma Basin, East Africa): planktonic foraminiferal evolutionary, geochemical and palaeoceanographic patterns. Sedimentology 64 (1), 252–285. https://doi.org/10.1111/sed.12331.
Petrizzo, M.R., 2019. A critical evaluation of planktonic foraminiferal biostratigraphy across the Coniacian-Santonian boundary interval in Spain, Texas, and Tanzania. In: Denne, R.A., Kahn, A. (Editors). Geologic Problem Solving with Microfossils IV, , Special Publication111. SEPM, pp. 186–198. https://doi.org/10.2110/sepmsp.111.04.
Petrizzo, M.R., Falzoni, F., Premoli Silva, I., 2011. Identification of the base of the lower-to-middle Campanian *Globotruncana ventricosa* Zone: Comments on reliability and global correlations. Cretaceous Research 32, 387–405. https://doi.org/10.1016/j.cretres.2011.01.010.
Petrizzo, M.R., Huber, B.T., Falzoni, F., MacLeod, K.G., 2020. Changes in biogeographic distribution patterns of southern mid-to high latitude planktonic foraminifera during the Late Cretaceous hot to cool greenhouse climate transition. Cretac. Res. 104547 https://doi.org/10.1016/j.cretres.2020.104547.
Pratt, L.M., 1985. Isotopic studies of organic matter and carbonate in rocks of the Greenhorn marine cycle. In: Pratt, L.M., Kauffman, E.G., Zelt, F.B. (Eds.), Fine-Grained Deposits and Biofacies of the Cretaceous Western Interior Seaway: Evidence of Cyclic Sedimentary Processes, Field Trip Guidebook, 4. Society of Economic Paleontologists and Mineralogists, pp. 38–48.
Pratt, L.M., Threlkeld, C.N., 1984. Stratigraphic significance of $^{13}C/^{12}C$ ratios in mid-Cretaceous strata of the Western Interior Basin. Mesozoic of Middle North America. Can. Soc. Petrol. Geol. Mem. 9, 305–312.
Premoli Silva, I., Sliter, W.V., 1995. Cretaceous planktonic foraminiferal biostratigraphy and evolutionary trends from the Bottaccione section, Gubbio, Italy. Palaeontographia Ital. 81, 2–90.
Premoli Silva, I., Sliter, W.V., 1999. Cretaceous paleoceanography: evidence from planktonic foraminiferal evolution. In: Barrera, E., Johnson, C.C. (Eds.), The Evolution of the Cretaceous Ocean-Climate System, Special Papers of the Geological Society of America, 332, pp. 301–328. https://doi.org/10.1130/0–8137–2332-9.301.
Premoli Silva, I., Erba, E., Salvini, G., Locatelli, C., Verga, D., 1999. Biotic changes in Cretaceous oceanic anoxic events of the Tethys. J. Foraminifer. Res. 29, 352–370.
Price, G.D., Sellwood, B.W., Corfield, R.M., Clarke, L., Cartlidge, J.E., 1998. Isotopic evidence for paleotemperatures and depth stratification of middle Cretaceous planktonic foraminifera from the Pacific Ocean. Geol. Mag. 135, 183–191.
Prokoph, A., Babalola, L.O., El Bilali, H., Olagoke, S., Rachold, V., 2013. Cenomanian–Turonian carbon isotope stratigraphy of the Western Canadian Sedimentary Basin. Cretac. Res. 44, 39–53.
Robaszynski, F., Caron, M., 1995. Foraminiféres planctoniques du Crétacé: commentaire de la zonation Europe-Méditerranée. Bull. Soc. Geol. Fr. 166, 681–692.
Robaszynski, F., Caron, M., Dupuis, C., Amédro, F., González Donoso, J.M., 1990. A tentative integrated stratigraphy in the Turonian of central Tunisia: formations, zones and sequential stratigraphy in the Kalaat Senan area. Bull. Centres Rech. Explor. Prod. Elf-Aquitaine 4 (1), 213–384.
Robaszynski, F., Caron, M., Amédro, F., Dupuis, C., Hardenbol, J., 1993. Le Cénomanien de la région de Kalaat Senan (Tunisie centrale): litho-biostratigraphie et interprétation séquentielle. Rev. Paléobiol. 12 (2), 351–505.
Robinson, S.A., Heimhofer, U., Hesselbo, S.P., Petrizzo, M.R., 2017. Mesozoic climates and oceans–a tribute to Hugh Jenkyns and Helmut Weissert. Sedimentology 64 (1), 1–15. https://doi.org/10.1111/sed.12349.
Robinson, S.A., Dickson, A.J., Pain, A., Jenkyns, H.C., O'Brien, C.L., Farnsworth, A., Lunt, D.J., 2019. Southern Hemisphere sea-surface temperatures during the Cenomanian-Turonian: Implications for the termination of Oceanic Anoxic Event 2. Geology 47 (2), 131–134.
Rullkötter, J., Littke, R., Radke, M., Disko, U., Horsfield, B., Thurow, J., 1992. Petrography and geochemistry of organic matter in Triassic and Cretaceous deep-sea sediments from the Wombat and Exmouth plateaus and nearby abyssal plains off Northwest Australia. In: von Rad, U., Haq, B.U., et al. (Eds.), Proceedings of the Ocean Drilling Program, Scientific Results 122, pp. 317–333. College Station, TX (Ocean Drilling Program).
Sadler, P.M., 2004. Quantitative biostratigraphy-Achieving finer resolution in global correlation. Annual Review Earth and Planetary Sciences 32, 187–213.
Sageman, B.B., Meyers, S.R., Arthur, M.A., 2006. Orbital time scale and new C-isotope record for Cenomanian – Turonian boundary stratotype. Geology 34, 125–128.
Scaife, J.D., Ruhl, M., Dickson, A.J., Mather, T.A., Jenkyns, H.C., Percival, L.M.E., Hesselbo, S.P., Cartwright, J., Eldrett, J.S., Bergman, S.C., Minisini, D., 2017. Sedimentary mercury enrichments as a marker for submarine large igneous province volcanism? Evidence from the Mid-Cenomanian event and Oceanic Anoxic Event 2 (Late Cretaceous). Geochem. Geophys. Geosyst. 18 (12), 4253–4275.
Schlanger, S.O., Jenkyns, H.C., 1976. Cretaceous oceanic anoxic events: causes and consequences. Geol. Mijnb. 55, 179–184.
Schlanger, S.O., Arthur, M.A., Jenkyns, H.C., Scholle, P.A., 1987. The Cenomanian-Turonian Oceanic Anoxic Event, I. Stratigraphy and distribution of organic carbon-rich beds and the marine $\delta^{13}C$ excursion. Geol. Soc. Lond. Spec. Publ. 26, 371–399.
Scholle, P.A., Arthur, M.A., 1980. Carbon isotope fluctuations in Cretaceous pelagic limestones: potential stratigraphic and petroleum exploration tool. AAPG Bull. 64, 67–87.
Schouten, S., Hopmans, E.C., Forster, A., van Breugel, Y., Kuypers, M.M.M., Damsté, J.S. S., 2003. Extremely high sea-surface temperatures at low latitudes during the middle Cretaceous as revealed by archaeal membrane lipids. Geology 31 (12), 1069–1072.
Schröder-Adams, C.J., Herrle, J.O., Selby, D., Quesnel, A., Froude, G., 2019. Influence of the high Arctic igneous province on the Cenomanian/Turonian boundary interval, Sverdrup Basin, High Canadian Arctic. Earth Planet. Sci. Lett. 511, 76–88.
Scopelliti, G., Bellanca, A., Coccioni, R., Luciani, V., Neri, R., Baudin, F., Chiari, M., Marcucci, M., 2004. High-resolution geochemical and biotic records of the Tethyan "Bonarelli Level" (OAE2, latest Cenomanian) from the Calabianca–Guidaloca composite section, northwestern Sicily, Italy. Palaeogeogr. Palaeoclimatol. Palaeoecol. 208, 293–317.
Scopelliti, G., Bellanca, A., Erba, E., Jenkyns, H.C., Neri, R., Tamagnini, P., Luciani, V., Masetti, D., 2008. Cenomanian–Turonian carbonate and organic-carbon isotope records, biostratigraphy and provenance of a key section in NE Sicily, Italy: palaeoceanographic and palaeogeographic implications. Palaeogeogr. Palaeoclimatol. Palaeoecol. 265 (1–2), 59–77.
Scotese, C.R., 2016. PALEOMAP PaleoAtlas for GPlates and the PaleoData Plotter Program, PALEOMAP Project. https://www.earthbyte.org/paleomap-paleoatlas-for-gplates/.
Shaw, A.B., 1964. Time in Stratigraphy. McGraw-Hill, New York, pp. 1–365.
Sinninghe Damsté, J.S., van Bentum, E.C., Reichart, G.J., Pross, J., Schouten, S., 2010. A CO_2 decrease-driven cooling and increased latitudinal temperature gradient during the mid-Cretaceous Oceanic Anoxic Event 2. Earth Planet. Sci. Lett. 293, 97–103.
Sissingh, W., 1977. Biostratigraphy of Cretaceous calcareous nannoplankton. Geol. Mijnb. 56, 37–65.
Smith, A.G., Barry, T., Bown, P., Cope, J., Gale, A., Gibbard, P., Gregory, J., Hounslow, M., Kemp, D., Knox, R., Marshall, J., Oates, M., Rawson, P., Powell, J., Waters, C., 2015. GSSPs, global stratigraphy and correlation. In: Smith, D.G., Bailey, R.J., Burgess, P.M., Fraser, A.J. (Editors). Strata and Time: Probing the Gaps in Our Understanding, , Special Publication404. Geological Society, London, pp. 37–67.
Strasser, A., Caron, M., Gjermeni, M., 2001. The Aptian, Albian and Cenomanian of Roter Sattel, Romandes Prealps, Switzerland: a high-resolution record of oceanographic changes. Cretac. Res. 22 (2), 173–199.
Takashima, R., Nishi, H., Hayashi, K., Okada, H., Kawahata, H., Yamanaka, T., Fernando, A.G., Mampuku, M., 2009. Litho-, bio-and chemostratigraphy across the Cenomanian/Turonian boundary (OAE 2) in the Vocontian Basin of southeastern France. Palaeogeogr. Palaeoclimatol. Palaeoecol. 273 (1–2), 61–74.
Tewari, A., Hart, M.B., Watkinson, M.P., 1996. Foraminiferal recovery after the mid-Cretaceous oceanic anoxic events (OAEs) in the Cauvery Basin, southeast India. Geol. Soc. Lond. Spec. Publ. 102 (1), 237–244.
Thurow, J., Brumsack, H.-J., Rullkötter, J., Littke, R., Meyers, P., 1992. The Cenomanian-Turonian Boundary event in the Indian Ocean – a key to understand the global picture. In: Duncan, R.A., Rea, D.K., Kidd, R.B., von Rad, U., Weissel, J.K. (Eds.), Synthesis of Results from Scientific Drilling in the Indian Ocean, AGU Geophys. Monogr., 70. American Geophysical Union, Washington, DC, pp. 253–274.
Trabucho Alexandre, J., Tuenter, E., Henstra, G.A., van der Zwan, K.J., van de Wal, R.S., Dijkstra, H.A., de Boer, P.L., 2010. The mid-Cretaceous North Atlantic nutrient trap: black shales and OAEs. Paleoceanography 25 (4), PA4201.
Tsikos, H., Jenkyns, H.C., Walsworth-Bell, B., Petrizzo, M.R., Forster, A., Kolonic, S., Erba, E., Premoli Silva, I., Baas, M., Wagner, T., Sinninghe Damsté, J.S., 2004. Carbon-isotope stratigraphy recorded by the Cenomanian–Turonian Oceanic Anoxic Event: correlation and implications based on three localities. J. Geol. Soc. Lond. 161, 711–719.
Turgeon, S.C., Creaser, R.A., 2008. Cretaceous Oceanic Anoxic Event 2 triggered by a massive magmatic episode. Nature 454, 323–326. https://doi.org/10.1038/nature07076.
van Helmond, N.A.G.M., Sluijs, A., Reichart, G.-J., Sinninghe Damsté, J.S., Slomp, C.P., Brinkhuis, H., 2014. A perturbed hydrological cycle during Oceanic Anoxic Event 2. Geology 42, 123–126.
Urquhart, E., Gardin, S., Leckie, R.M., Wood, S.A., Pross, J., Georgescu, M.D., Ladner, B., Takata, H., 2007. A paleontological synthesis of ODP Leg 210, Newfoundland Basin. In: Tucholke, B.E., Sibuet, J.-C., Klaus, A. (Eds.), Proceedings Ocean Drilling Program Scientific Results 210, pp. 1–53. https://doi.org/10.2973/odp.proc.sr.210.115.2007. College Station, TX.
van Bentum, E.C., Reichart, G.J., Forster, A., Sinninghe Damsté, J.S., 2012. Latitudinal differences in the amplitude of the OAE-2 carbon isotopic excursion: pCO_2 and paleo productivity. Biogeosciences 9 (2), 717–731.
van Helmond, N.A., Sluijs, A., Papadomanolaki, N., Plint, A.G., Gröcke, D., Pearce, M., Eldrett, J.S., Trabucho-Alexandre, J., Walaszczyk, I., van de Schootbrugge, B., Brinkhuis, H., 2016. Equatorward phytoplankton migration during a cold spell within the Late Cretaceous super-greenhouse. Biogeosciences 13 (9), 2859–2872.

Voigt, S., Erbacher, J., Mutterlose, J., Weiss, W., Westerhold, T., Wiese, F., Wilmsen, M., Wonik, T., 2008. The Cenomanian–Turonian of the Wunstorf section (North Germany): global stratigraphic reference section and new orbital time scale for Oceanic Anoxic Event 2. Newsl. Stratigr. 43, 65–89.

Voigt, S., Gale, A.S., Flögel, S., 2004. Midlatitude shelf seas in the Cenomanian-Turonian greenhouse world: temperature evolution and North Atlantic circulation. Paleoceanography 19, PA4020. https://doi.org/10.1029/2004PA001015.

Voigt, S., Gale, A.S., Voigt, T., 2006. Sea-level change, carbon cycling and palaeoclimate during the Late Cenomanian of northwest Europe; an integrated palaeoenvironmental analysis. Cretac. Res. 27, 836–858.

Von Strandmann, P.A.P., Jenkyns, H.C., Woodfine, R.G., 2013. Lithium isotope evidence for enhanced weathering during Oceanic Anoxic Event 2. Nat. Geosci. 6 (8), 668–672.

Watkins, D.K., Bergen, J.A., 2003. Late Albian adaptive radiation in the calcareous nannofossil genus *Eiffellithus*. Micropaleontology 49, 231–252.

Wendler, I., 2013. A critical evaluation of carbon isotope stratigraphy and biostratigraphic implications for Late Cretaceous global correlation. Earth Sci. Rev. 126, 116–146.

Wendler, I., Huber, B.T., MacLeod, K.G., Wendler, J.E., 2013. Stable oxygen and carbon isotope systematics of exquisitely preserved Turonian foraminifera from Tanzania – understanding isotopic signatures in fossils. Mar. Micropaleontol. 102, 1–33.

Westermann, S., Caron, M., Fiet, N., Fleitmann, D., Matera, V., Adatte, T., Föllmi, K.B., 2010. Evidence for oxic conditions during Oceanic Anoxic Event 2 in the northern Tethyan pelagic realm. Cretac. Res. 31, 500–514.

Wilson, P.A., Norris, R.D., Cooper, M.J., 2002. Testing the Cretaceous greenhouse hypothesis using glassy foraminiferal calcite from the core of the Turonian tropics on Demerara Rise. Geology 30, 607–610.

Wonders, A.A.H., 1992. Cretaceous planktonic foraminiferal biostratigraphy, Leg 122, Exmouth plateau, Australia. Proc. Ocean Drill. Program Sci. Results 122, 587–599.

Zheng, X.Y., Jenkyns, H.C., Gale, A.S., Ward, D.J., Henderson, G.M., 2013. Changing ocean circulation and hydrothermal inputs during Ocean Anoxic Event 2 (Cenomanian–Turonian): evidence from Nd-isotopes in the European shelf sea. Earth Planet. Sci. Lett. 375, 338–348.